Engineering Failure Analysis 94 (2018) 121–144

Contents lists available at ScienceDirect

Engineering Failure Analysis

journal homepage: www.elsevier.com/locate/engfailanal

Fatigue analysis of a railway bridge based on fracture mechanics and local modelling of riveted connections

Fernando Marques[a,*], José A.F.O. Correia[a,b], Abílio M.P. de Jesus[a,b], Álvaro Cunha[a], Elsa Caetano[a], Augusto A. Fernandes[a,b]

[a] Faculty of Engineering, University of Porto (FEUP), R. Dr. Roberto Frias, 4200-465 Porto, Portugal
[b] INEGI, R. Dr. Roberto Frias, 4200-465 Porto, Portugal

ARTICLE INFO

Keywords:
Riveted railway bridge
Fatigue assessment
Finite element models
Local models
Fracture mechanics
Random loading

ABSTRACT

In the context of fatigue evaluation of riveted railway bridges, cross-girder to main beam connections are frequently critical details. Secondary effects, such as out-of-plane bending and dynamic amplifications due to the proximity to loading paths which in the case of old bridges were not taken into account in the original design, may lead to severe increase of fatigue damage.

The fatigue assessment of old riveted railway bridges has been addressed in the last years by developing local models of critical riveted joints that are linked to global models. This local-global modelling approach aims at evaluating local secondary stresses. Former fatigue probabilistic analyses of riveted joints have been focused on resistance variability rather than on loading/stresses (actions) variability.

In this paper a probabilistic procedure to include the variability of loading in the fatigue analysis of complex riveted joints of railway bridges is proposed assuming loading as a random variable. Local finite element models were developed and later coupled with the global model in order to obtain the real stresses associated to real trains crossing the bridge. To reduce computational time, the results obtained from these local models were inputted in a Linear Fracture Mechanics model, supported by Paris fatigue crack propagation law. Monte Carlo simulation technique was applied to calculate the fatigue reliability of an old riveted railway bridge, considering traffic records from previous studies on the bridge.

1. Introduction

In the context of fatigue evaluation and for riveted railway bridges, cross-girder to main beam connections are, in general, the critical details [1, 2]. Secondary effects as is the case of out of plane bending and dynamic amplifications due to their proximity to the loading paths that were, in the case of old bridges, not taken into account in the design may lead to severe increase of the fatigue damage. Furthermore, the variability of the loading is not so often included in the analysis.

In the context of fatigue assessment of old riveted railway bridges, several authors have developed local models of critical riveted joints that were included in global models in order to evaluate local secondary stresses [3–6]. However, the complete stress history was not included in the analysis.

Refined fatigue assessment of old riveted bridges using complex finite element models is very difficult due to the large amount of stress cycles required to calculate fatigue damage, since it is a case of typical variable amplitude stress [7]. Former fatigue

* Corresponding author.
E-mail address: dec11014@fe.up.pt (F. Marques).

https://doi.org/10.1016/j.engfailanal.2018.07.016
Received 30 January 2018; Received in revised form 5 June 2018; Accepted 20 July 2018
Available online 27 July 2018
1350-6307/

probabilistic analyses of riveted joints rarely accounts for the stress range variability.

Historically, the economic development has been always associated with the construction of railway lines, with subsequent increase of traffic, vehicle axle loads and speed. Therefore, old railway metallic bridges, in many cases with more than one hundred years, have been pushed over the years to carry out heavier vehicles and endure higher velocities than allowed by the original design. In addition, the cumulated degradation due to corrosion and fatigue, contributes to an increased concern about their safety.

This paper proposes a procedure to include the variability of loading into a probabilistic methodology aiming the fatigue analysis. The loading is assumed as a random variable. Since the shape function of Paris law depends on the loading, this aspect must be taken into account in the proposed procedure. Furthermore, local finite element models using volume elements and contact elements are developed and later coupled with the global model in order to obtain the real stresses associated with trains crossing the bridge. To reduce computational time, the results obtained from these local models are used in a Linear Fracture Mechanics model. In particular, several shape functions are obtained from these numerical studies and later included in the Paris law [8]. Monte Carlo simulation technique is used to calculate the fatigue reliability for an old riveted railway bridge. Results obtained from previous studies on the traffic evaluation of this bridge are included in the model [9]. The stress data obtained from a long term monitoring campaign is used to calculate the load function which allows the random generation of each train crossing on the bridge. The statistical characteristics of the random variables related to the material are obtained from an experimental study developed in other research work [9].

Advanced local Finite Element Models (FEM) models are developed in *APDL (ANSYS Parametric Design Language)* programming language available in *Ansys* software in order to allow the parameterization of the characteristics of the critical riveted connections. The contact between rivets and steel plates are included in these models using numerical algorithms that allow the simulation of friction contact between several structural elements. Since it is extremely complex to simulate in this local model all the stress histories related to each real train, the numerical model is used to calculate two shape functions corresponding to two characteristic trains with the highest and lowest axle loads. The real shape function (corresponding to all the real trains) has to be related to, or has to be a combination of the previous referred shape functions. Therefore, a genetic algorithm is implemented in order to find the shape function which minimizes the fatigue life.

2. Description of the bridge – case study

The study presented in this paper is supported by a case study which is the Portuguese riveted railway Trezói bridge. The Trezói Bridge (see Fig. 1) is located in the international “Beira Alta” railway line that links Portugal to Spain, at the km 62, north of Mortágua, in the village of Trezói. The bridge was constructed as part of a project to replace existing bridges in the “Beira Alta” railway line, carried out during the decade of 1950’s, and was opened to traffic in August 1956. The project was funded by the Marshall Plan, and the conception, manufacture and mounting, together with 6 other bridges of larger span of the same line, was of the responsibility of the German House Fried Krupp.

This steel riveted bridge has three spans; their lengths are 48 m for the central span and 39 m for the other two spans. The total length of the bridge is 126 m. Two inverted Warren truss girders that forms the metallic deck of the bridge are 5.68 m height. The girder panels are 6.50 m wide in the central span and 6.00 m in the end spans. Two trapezoidal shape trusses acting as columns and two granite masonry abutments transmit the loads supported by the structure to the foundations. The bridge has a constant width of 4.40 m throughout its length. Fig. 2 illustrates the general geometry of the bridge.

The cross girders, as well as the stringers resting on them, were built using “I-shaped” sections. The cross girders are 71 cm height and are connected to the lateral vertical elements with riveted plates as shown in Fig. 2. The chords and diagonals of the truss girders are formed by double “U-shape” sections.

The bearing supports of the superstructure are metallic and allow free rotations in the structure plane. At the east support, the longitudinal displacements are constrained, while at the west support deformations caused by longitudinal horizontal forces (thermal actions, braking forces, etc.) are allowed.

The stringers are symmetrically placed with respect to the rails which is a fortunate conception option since non-symmetrical rails normally induce higher secondary stresses in the web of the stringers.

Fig. 1. The Trezói bridge.

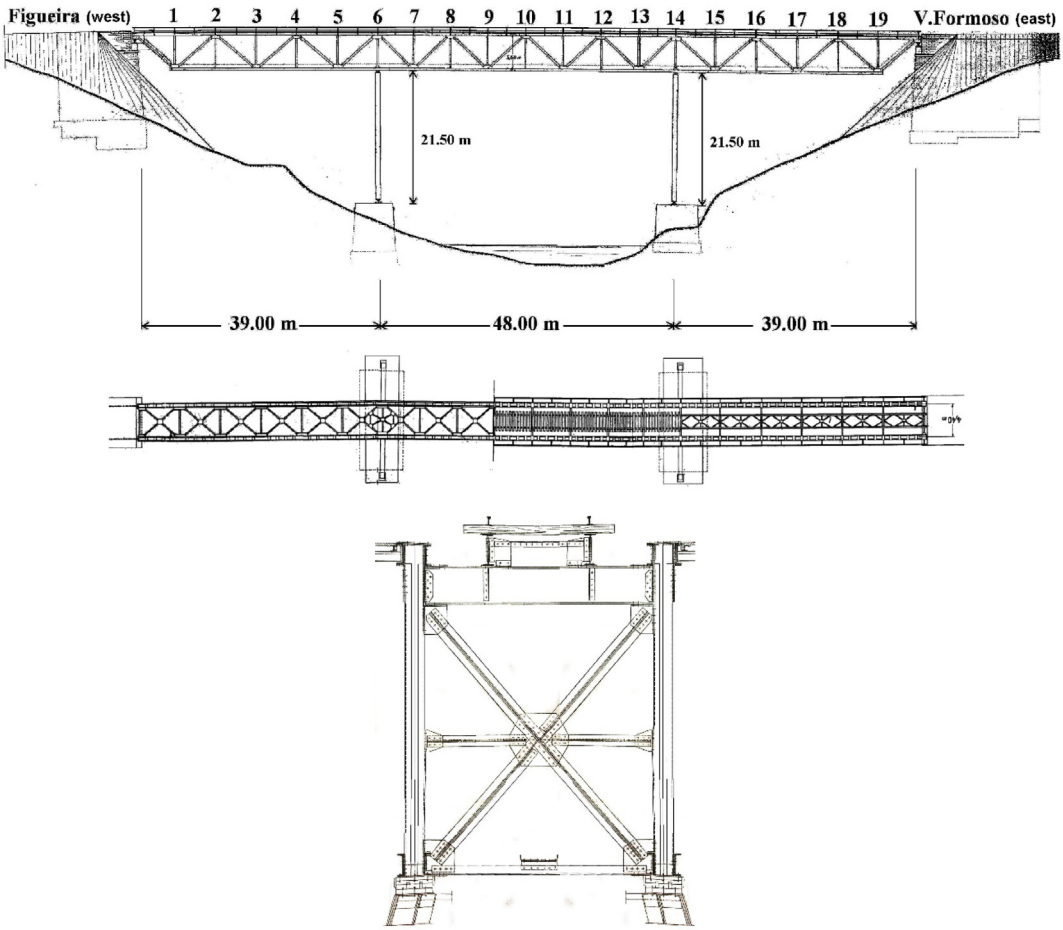

Fig. 2. Elevation, plan view and cross section of the Trezói bridge.

3. Identification of fatigue critical elements

Fatigue analysis of railway bridges has to take into account several phenomena in order to correctly identify the critical elements. For example, local vibrations may have a significant influence in the fatigue damage [2]. In this context, for the bridge analysed in this work, a previous study was conducted in order to evaluate the global and local dynamic behaviour. This study is described in detail in [9]. However, for the sake of completeness, this analysis is briefly summarized in this section.

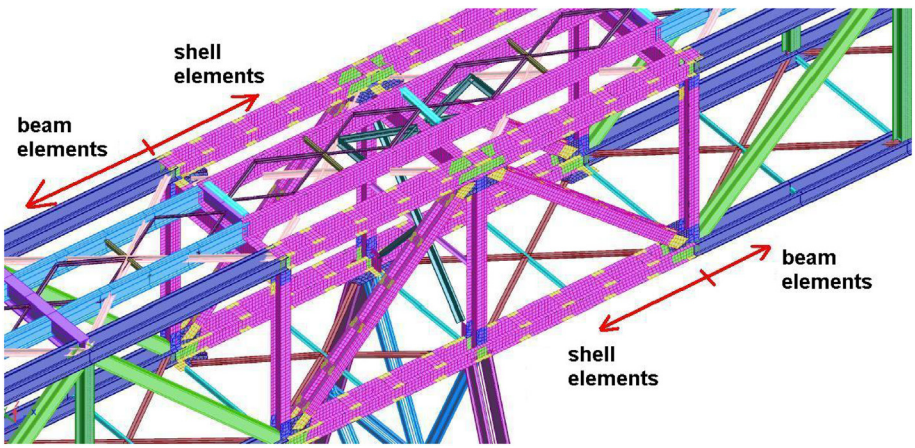

Fig. 3. FEM model detail using beam and shell elements – local view above the main columns [9].

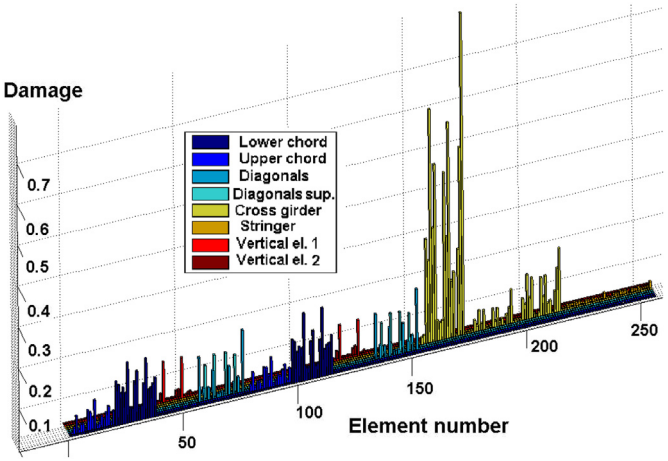

Fig. 4. Fatigue damage index for all structural elements for a real traffic scenario [9].

Numerical studies were conducted based on FE models to evaluate the dynamic behaviour of the bridge using a discretisation of the structure with 3D beam elements, truss elements and shell elements [9] (see Fig. 3). Trains crossing the bridge at a wide range of velocities were simulated and the resulting nominal stresses on members were used to evaluate the fatigue damage index, based on Miner's rule [10]. Furthermore, a monitoring campaign using strain gauges was implemented in order to validate the numerical models and to obtain real stresses due to the crossing of trains.

Both numerical and experimental studies allowed to conclude that the cross-girders were the critical elements in terms of fatigue behaviour as can be seen in Fig. 4, where the damage for each structural element of the bridge can be observed. These calculations were made using the class 71 S-N curve from the EN1993-1-9 standard [11].

4. Fatigue analysis methodology based on fracture mechanics and local modelling of critical connections

4.1. Implemented methodology

The residual fatigue life of the Trezói bridge is estimated in this paper using an alternative procedure to the S–N approach referred in previous section and applied in previous works [9]. Fracture Mechanics and the methodology proposed by Massareli et al. [12] were implemented using routines developed in *Matlab*. The Paris Law (Eq. (1)) and the Monte Carlo simulation method are central in this methodology. The statistical properties of material characteristics (C and m), stress ranges ($\Delta\sigma$), and initial and critical crack lengths (a_{ini} and a_{crit}) are taken into account to calculate fatigue lives. The crack length variation, Δa, per cycle and the stress intensity factor variation per cycle, ΔK, can be calculated using Eqs. (2) and (3). Combining these two equations into Eq. (4) and summing up all Δa within a stress block b, Eq. (5) is obtained. In this context, a stress block is associated with a loading event which corresponds to the crossing of a single train or to the crossing of a group of several trains. Eq. (5) is valid as long as the crack length remains constant during this loading event (stress block). This assumption is, in general, valid for high cycle fatigue, which is the common situation in bridges [12]. In Eq. (5), b stands for the block loading and n represents the number of cycles in the block.

$$\frac{da}{dN} = C(\Delta K)^m \tag{1}$$

$$\Delta a = C(\Delta K)^m \tag{2}$$

$$\Delta K = Y(a)\Delta\sigma\sqrt{\pi a} \tag{3}$$

$$\Delta a = C[Y(a)\Delta\sigma\sqrt{\pi a}]^m \tag{4}$$

$$[\Delta a]_b = \left[\sum_{i=1}^{n} \Delta a_i\right]_b = C[Y(a)\sqrt{\pi a}]^m|_b \sum_{i=1}^{n} \Delta\sigma_i{}^m \tag{5}$$

A damage stress function $h(B_N(w))$ is proposed in [12] as:

$$h[B_N(w)] = \sum_{i=1}^{n} (\Delta\sigma_i)^m \tag{6}$$

In order to obtain the stress range included in this equation it is necessary to implement a cycle counting algorithm. The Rainflow algorithm [13] was implemented in a routine developed in *Matlab*. Hence, for each stress history corresponding to each real train, this algorithm is used to calculate the damage stress function. The number of blocks to failure B_f is related to $h[B_N(w)]$ by:

$$B_f = \int_{a_{ini}}^{a_{crit}} \frac{da}{C(Y(a)\sqrt{\pi a})^m}\left[\frac{1}{h[B_N(w)]}\right] \tag{7}$$

Due to the nonlinearity of the stress intensity factor, a closed form integration is difficult to obtain. However, for this model, the crack growth per block loading could be approximated by Eq. (8):

$$a_{j+1} = a_j + C(Y(a_j)\sqrt{\pi a_j})^m h_j[B_N(w)] \tag{8}$$

Based on the assumption that C and m are constants, the crack length at the end of the j^{th} loading block, can be calculated using Eq. (8) where the stress function (h_j) can be associated, for example, to the previous train crossing (increment j). In this equation, a_j is the crack length at increment j and $Y(a_j)$ is the value of the shape function for a_j.

In the proposed procedure, the materials parameters and the stress function itself are considered random variables. Consequently, the Monte Carlo simulation method can be implemented in this case. If $h(BN(w))$, C and m are random variables, the crack length for simulation i, can be obtained from.

$$a_{j+N} = a_j + C_i(Y(a_j)\sqrt{\pi a_j})^{m(i)} h_j[B_N(w)] \tag{9}$$

The calculations of crack length are stopped when the crack length leads to a maximum stress intensity factor, corresponding to the material toughness K_c, as presented by Eq. (10):

$$a_{crit} = \frac{1}{\pi}\left(\frac{K_C}{Y \cdot f_y}\right)^2 \tag{10}$$

The critical crack size depends on the applied stress, increasing the critical crack size with decreasing applied stress. Since the applied stress is considered a random variable, is not possible to specify a constant/deterministic critical crack size. The integration of the crack growth law considering loading blocks composed of cycles with variable amplitude loading, does not allow the establishment of unique critical crack size for each block increment, since the critical crack size would depend on the maximum stress present in the block, which is also a random variable. Also, due to the possibility of occurring high stresses at the rivet holes vicinity (stress concentration), it was assumed the critical crack size defined by a maximum stress corresponding to the material yield stress, f_y. In previous equation, K_c and f_y properties are assumed random variables. Since the characteristics of the cracks hidden by the rivet heads are not fully controlled, this equation based on the yield stress aims to obtain conservative results, and preferably considering critical, those cracks growing beyond the rivet heads and detectable by inspections.

Fig. 5 presents the workflow that summarizes the methodology implemented in this paper to assess the fatigue behaviour of the Trezói bridge riveted joint. The workflow was automated by means of routines developed in *Matlab*.

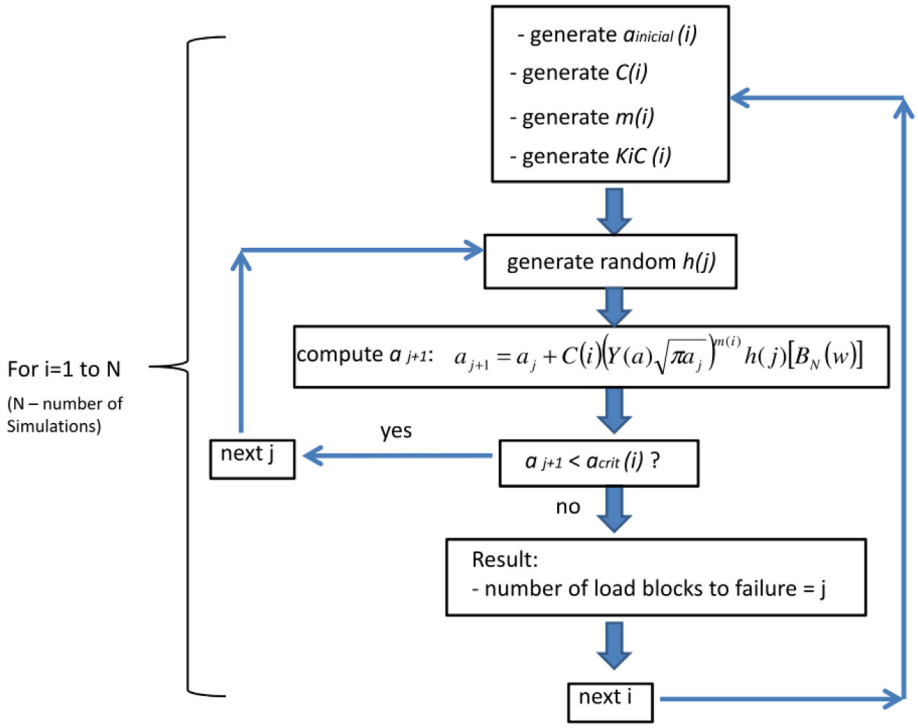

Fig. 5. Workflow based on the methodology proposed by Massareli et al. [12].

For each simulation i, the following random variables are generated: the initial crack length $a_{initial}(i)$, the material properties $C(i)$ and $m(i)$ and the fracture toughness $K_c(i)$. For each simulation i, the damage stress function is randomly generated j times and the crack length a_{j+1} is replaced in a_j until the crack length is equal to the critical length ($a_{crit}(i)$).

For each simulation i, the number of loading blocks to failure ($h(j)$) j is recorded. Therefore, depending on the information used to calculate the damage stress function, j may be the total number of trains to failure (if the stress spectra used is related to each train), j may also be the total number of days to failure (if daily stresses were used) or the total number of months to failure (if monthly records are used).

As proposed in [12], to reduce the computational demands of the single block iteration, the model makes the following assumptions:

1. The crack size will remain reasonably constant over a period of consecutive, multiple blocks, so that there is no significant increase in the $C_i(Y(a_j)\sqrt{\pi a_j})^{m(i)}$ term of Eq. (9) during this period.
2. The cumulative effect of multiple random values of the damage stress function can be approximated by a single normally distributed random value by employing the central limit theorem (CLT) of probability.

In this work, a sensitive analysis on the validity of the 2nd assumption is presented in Section 4.4.3. It was concluded in that section that the monthly stress block function is sufficient to accurately calculate the crack growth. Furthermore, given the relatively large fatigue propagation lifetimes of most structural cracks, this assumption seems fairly reasonable.

4.2. Random variables evaluation

The random variables simulated in this fatigue damage assessment procedure are the stress block function, the fatigue crack propagation constants C and m, the initial crack length a_i and the fracture toughness K_C (which dictates the critical crack length).

Laboratory tests were conducted by Ribeiro et al. [14] in order to measure the fatigue crack growth rates and to calculate the

a)

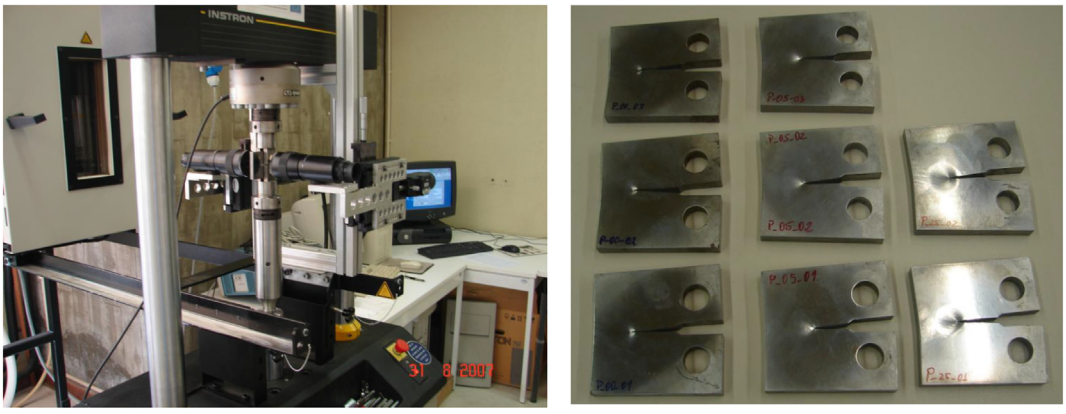

b)

Fig. 6. Fatigue crack propagation tests: a) location of the original bracing removed from the bridge; b) optical system for crack growth measurements and CT specimens after testing [14].

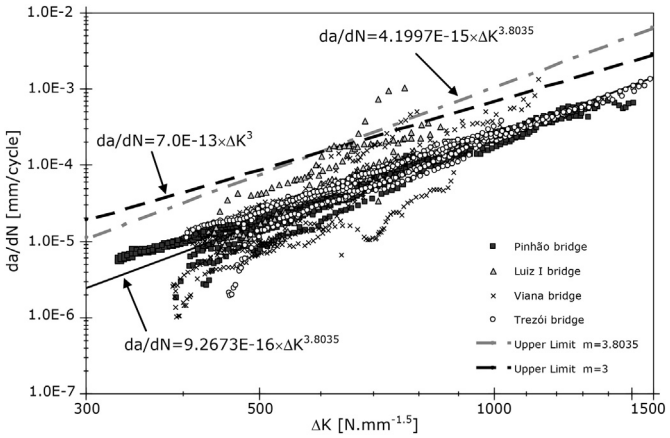

Fig. 7. Fatigue crack propagation data from various Portuguese bridge materials [14, 16].

material constants C and m in accordance with ASTM E647 standard [15]. For that purpose, a bracing was removed from the bridge and replaced by a bolted one in order to test the real material from the bridge as can be observed in Fig. 6a). Eight Compact Tension (CT) specimens were obtained from that structural element as can be observed in Fig. 6b). The results from these tests are compared with results from other old metallic bridges in Portugal and are presented in Fig. 7.

It was concluded that the Trezói bridge has similar material characteristics to the other three bridges analysed. Applying a linear regression to the log-log experimental data from Trezói bridge, resulted the following expression for the fatigue crack propagation rates:

$$\frac{da}{dN} = 4.5273 \times 10^{-15} \Delta K^{3.575} \tag{11}$$

The previous results are not sufficient to estimate the statistical properties of the parameters of the Paris relation representing the material of the Trezói bridge [17]. For simulation purpose, the mean value for C was assumed equal to 4.5273×10^{-15} [da/dN in mm/cycle and ΔK in $N.mm^{-1.5}$] and for m the mean value was assumed equal to 3.575. A Gaussian distribution was assumed and the corresponding standard deviations were obtained from a similar study performed in the USA [18], where a significant number of roadway bridges were studied. Concerning the crack size, also assumed as a random variable, several criteria have been proposed in the literature. Its magnitude is normally within the range of 0.1 mm to 1.0 mm, the value of 0.5 mm being a very common proposal [19] [20] [21]. The initial crack length (a_i) and standard deviation values were also obtained from reference [18].

The mean value of the fracture toughness (K_C) was also obtained from the laboratory tests developed in [22] where Charpy tests were conducted in 16 specimens obtained from the original material of Trezói bridge. In order to calculate the fracture toughness, K_C, from the experimental Charpy V-Notch energy (CVN), Eq. (12) proposed by Barsom and Rolfe was used:

$$\left(\frac{K_C}{\sigma_{ced}}\right)^2 = \frac{5}{\sigma_{ced}}\left(CVN - \frac{\sigma_{ced}}{20}\right) \tag{12}$$

The results are reproduced in Fig. 8.

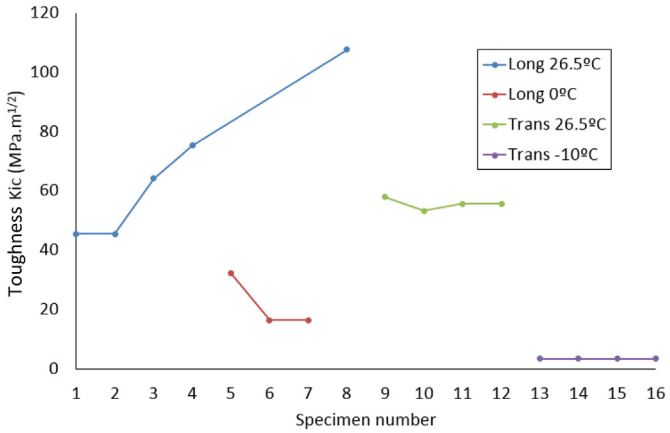

Fig. 8. Results from the Charpy notch test of the material of Trezói bridge.

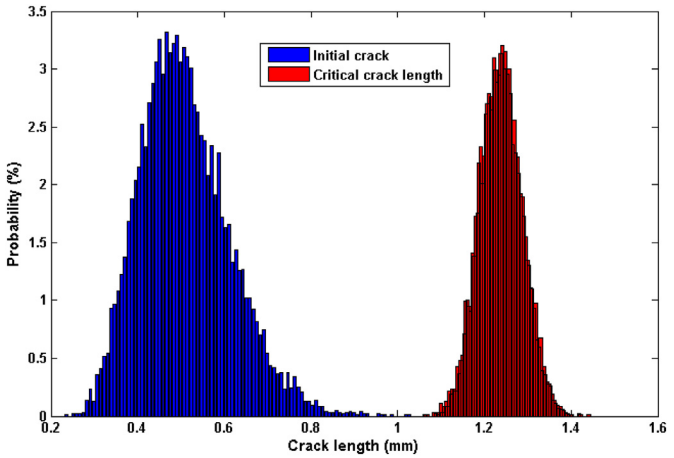

Fig. 9. Initial and critical crack length histograms.

These results were used to calculate the distribution of the critical crack length using the Eq. (10). As can be observed, the critical crack length is dependent on the shape function Y, which is dependent on the length of the crack. Therefore, in order to calculate a_{crit}, several iterations are made using a routine developed in *Matlab*.

Furthermore, the characterization of the shape function depends on the geometry of the structural detail and loading spectra. Several shape functions were investigated in Section 4.3 in order to conclude about their influence on a_{crit} and on the fatigue life. These results are presented in Sections 4.4.2 and 4.4.5, respectively.

In this work, the standard deviation of the initial and critical crack size were also obtained from [18]. In Fig. 9, the histograms of the initial and critical crack length (using the shape function defined in Section 4.3) calculated with a reference shape function (see Section 4.3.8) are presented and the corresponding mean and standard deviation are presented in Table 1.

The damage stress function statistical properties were estimated using a long term monitoring campaign described in references [9] [23], where strain gauges were used to measure strains in the cross-girders in the period between November 2011 and December 2014.

In Fig. 10, the histogram of this random variable is presented. The value of $h(w)$ was calculated for each real train measured over the time period previously referred. Due to the complex histogram obtained, a non-parametric distribution was fitted to the results. As described in [24], a kernel density estimator of a unknown probability density function f of a given n values of x can be obtained from:

$$\widehat{f_h}(x) = \frac{1}{n}\sum_{i=1}^{n} K_h(x - x_i) = \frac{1}{nh}\sum_{i=1}^{n} K\left(\frac{x - x_i}{h}\right) \tag{13}$$

where x_i are the data values, h is the bandwidth and K is the kernel.

To choose the optimal parameters for this case, a sensitive analysis was made. Since the kernel bandwidth controls the smoothness of the probability density function, a significant influence on the results was expected. As can be observed in Fig. 11a), the blue curve corresponding to a bandwidth of 2.08796E6 is "undersmoothed" since it contains too many variations arising, for example, within the range of $h(w) = [1.5E7; 3.0E7]$; the conclusion obtained is that this bandwidth is too small. The curves corresponding to bandwidths 6.08796E6 and 7.99923E6 are "oversmoothed" since using these bandwidths the estimator does not capture much of the underlying data values. This is particularly true for the same range referred previously. Therefore, a bandwidth of 4.087796E6 was chosen since it appears to capture the variability of the data without introducing discrepancies.

In Fig. 11b) the influence of the kernel can be observed. It was concluded that, in this case, the change in the kernel function has a small influence in the results.

In Fig. 12, a comparison is made between original and randomly generated values of $h(B(w))$. An additional numerical restriction was introduced in order to avoid obtaining negative values. As can be observed, there is a good agreement between the results, hence increasing the confidence in the probability density function adopted for this variable.

Table 1
Statistical characteristics of initial and critical crack length.

Random variable	Mean	Standard deviation	Probability distribution
Initial crack length, a_i (mm)	0.5	0.201	Lognormal
Critical crack length, a_c (mm)	1.24	0.049	Normal

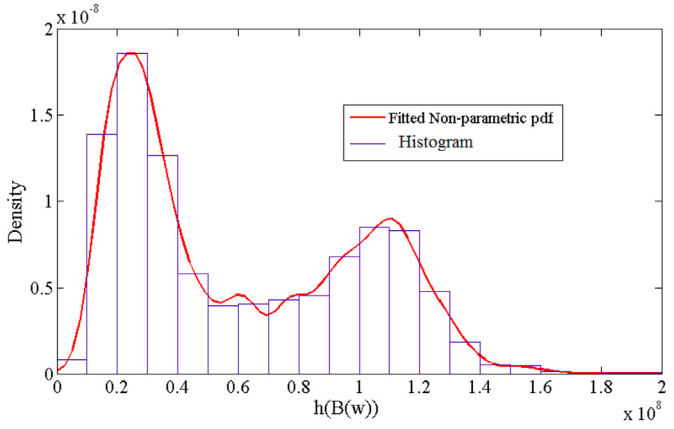

Fig. 10. Load function histogram with fitted pdf.

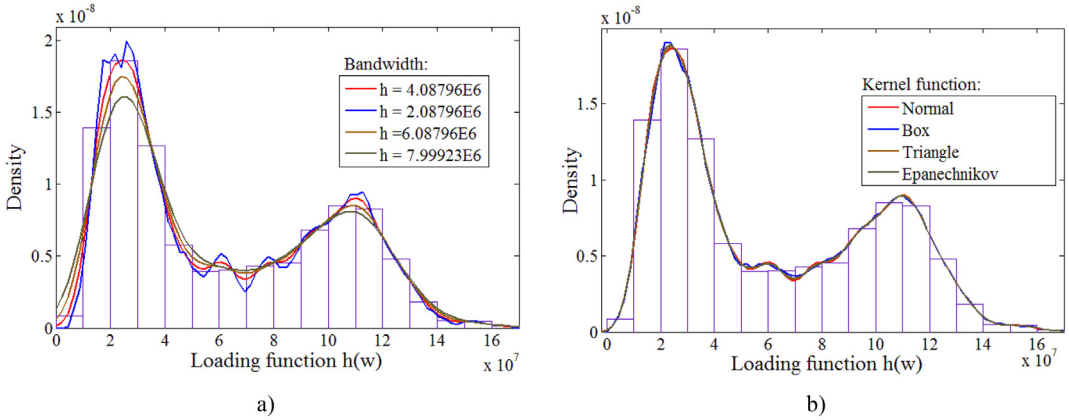

Fig. 11. Sensitive analysis for the parameters used in the non-parametric density function estimation of loading function: a) bandwidth variation; b) kernel function.

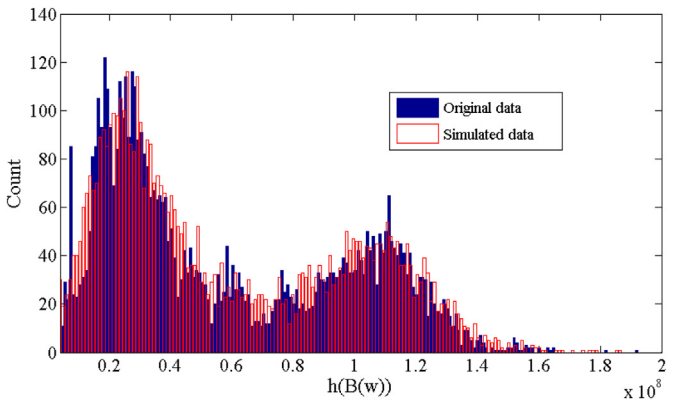

Fig. 12. Comparison between original and simulated $h(B(w))$ histograms.

4.3. Shape function evaluation using a local numerical model of a critical detail

4.3.1. Introduction

For the case of simple geometries, the shape function *Y(a)* may be obtained from literature (for example, see reference [25]). However, due to the complexity of the riveted joints being studied, this would imply an inaccurate solution if one of the analytical expressions in [25] were chosen for the analysis. To avoid this difficulty, the estimation of the shape function can be made using finite element models where the crack is simulated and the stress intensity factors are calculated numerically for each crack length. In this

context, local numerical models were developed in order to calculate the shape function associated to the complex geometry of the riveted connection between the cross-girder and the remaining structural elements.

As presented in Section 4.1, the stress intensity factor can be obtained using Eq. (3) and the shape function *Y(a)* can be obtained using Eq. (13):

$$Y = \frac{K}{\sigma\sqrt{\pi a}} \tag{14}$$

The stress intensity factor, as the shape function, depends on the loading, the crack shape, the fracture mode and the geometry of the solid. In this section, several shape functions were investigated in order to evaluate their influence on the fatigue life.

The ideal approach to this problem would be to simulate the crack growth using a local FEM model [26, 27] and the real variable amplitude loading from the entire period of the long term monitoring campaign. However, such approach is impracticable due to the computational resources it requires since a large amount of data is involved and due to the complexity of the local model, which implies a non-linear analysis due to the contact algorithm used and due to the necessity to calculate the stress intensity factors for each crack increment [28].

In this section, a simplified approach is proposed to avoid this problem. Two shape functions are calculated for the two extreme trains in terms of axle loads [9, 23]. Then, a genetic algorithm is used to minimize the fatigue life by changing the parameters of the shape function built using as basis the previous two calculated and several other shape functions obtained from literature. This procedure allows finding the worst case scenario within the two boundaries obtained by the two trains previously referred.

4.3.2. Description of the critical structural detail

In the research briefly presented in Section 3, it was concluded that the critical elements in terms of fatigue evaluation are the cross-girders. In particular, the riveted detail located at the top flange of these elements is decisive in terms of fatigue cracking. The location and geometry of this structural detail is presented in Fig. 13a and b.

Taking these results into consideration, two local finite element models were developed. In order to evaluate stress concentration factors and to evaluate the potential crack initiation location, an uncracked model was developed. The effects of the contact between the rivets and the top flanges and the contact between the flanges and the gusset metallic plate were taken into consideration using solid elements and 3D surface-to-surface contact pairs, following the recommendations in references [29, 30]. Twenty-noded elements of the type “SOLID95” [30] were used and the effect of contact between the rivet's shank and the holes, between the head of the rivets and the steel plates, and between the steel plates were included.

A second model with an explicit crack was also developed in order to calculate the stress intensity factors. For that purpose, the virtual crack closure technique was implemented in the *Ansys* APDL programming language. The local finite element model of the most critical connection location is depicted in Fig. 14. This particular connection is composed by the cross-girder, the diagonal, the top beam and one bracing. All rivets show a 25 mm diameter; contact and friction between the individual parts of the connection as well as the rivet clamping force were included in the model. In contrast to the global bridge model, the local model permits investigation of the fatigue damage of the individual elements of the connection. This model also allows the local stiffness of the connection and secondary effects to be accounted for.

In Fig. 15, the meshed model is presented. The mesh refinement and contact properties were chosen in accordance with the recommendations presented in [26] and the research developed in [31]. This FEM model is composed by 565,998 elements and

a) b)

Fig. 13. Local view of the cross-girders at the extremity support: a) global view; b) top view of rivets at the top flange.

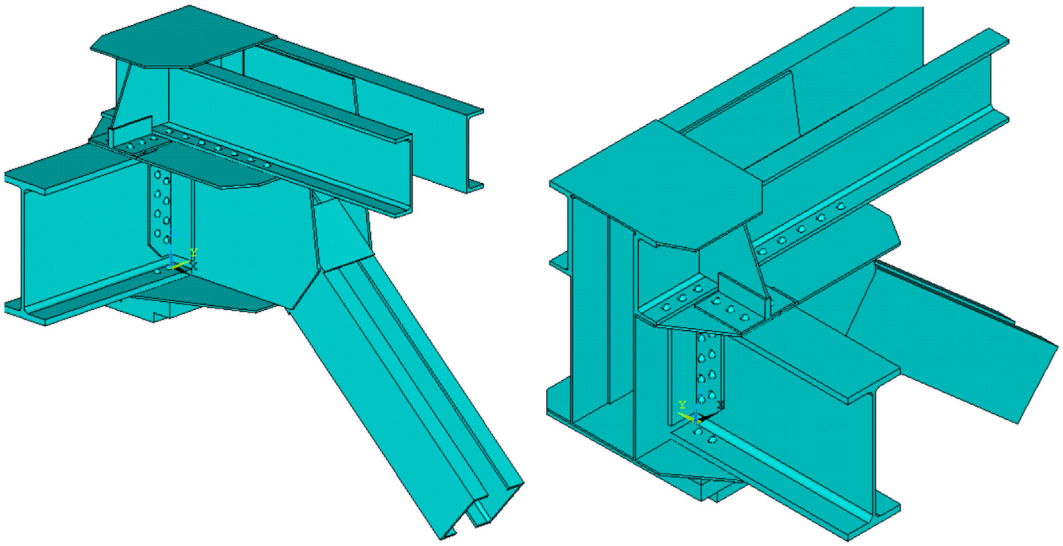

Fig. 14. Geometry of the primary local FEM model.

115,791 nodes.

Linear elastic material properties were assumed with a Young modulus of 198.49 GPa and a Poisson coefficient of 0.3, in accordance with the tests developed in [32–35].

The clamping force induced by the rivets was simulated using a negative temperature variation in order to result a reduction of the length of the rivet shank. A thermal expansion coefficient of 10^{-5} was imposed in the longitudinal/axial direction of the rivets, and null expansion in the other perpendicular directions, in order to correctly simulate the clamping in only one direction (orthotropic thermal properties). Wilson and Thomas [32] proposed a clamping stress equal to 80% of the yield stress. As referred previously, Ribeiro et al. [14] conducted laboratory tests which included tension tests leading to an average yield stress of 410 MPa and an average rupture stress of 464 MPa. Taking into account these results, the clamping stress would be within the range of 313 MPa to 322 MPa.

4.3.3. Contact properties

In order to simulate the contact between the components of the detail, a surface-to-surface and flexible-to-flexible contact behaviour was used [36, 37]. The contacting surface pairs where modelled with contact (CONTA174, [30]) and target elements (TARGET170, [30]) and were applied in the interfaces between the rivets heads and the side surfaces of the plates, the rivet shank and the surface of the hole and between the surfaces of the plates. The Coulomb friction model was used and friction coefficients of 0.0, 0.3 and 0.5 were considered [38].

4.3.4. Boundary conditions

The displacements obtained from the global FEM model were applied to key nodes located at the centroid of each section (see Fig. 16). In order to successfully perform this, avoiding stress concentration due to point loads, a special constraint was implemented using the contact algorithms. The keypoints and the surface of each elements form an advanced contact pair in which the section areas follow the same displacements and rotations of the corresponding keypoint. Furthermore, the support was also simulated using contact pairs. In this case, a keypoint was created at the centre of rotation of the support. This approach is equivalent to the simulation using “rigid links”. The boundary condition at the support was also simulated using contact pairs.

4.3.5. Loading conditions

The traffic and loading conditions were obtained from the B-WIM algorithm presented in reference [9, 23]. The information of the real trains obtained was then used to calculate stresses and displacements taking into account the dynamic properties of the global numerical model [23], and using the moving loads technique [9, 39]. The displacements and rotations were calculated at the nodes in exact correspondence with the local FEM model section keypoints as can be observed in Fig. 17.

Due to the high complexity of loading and the high number of real trains crossing the bridge it is not possible to simulate the real loading conditions in the local numerical model. Therefore, two real measured trains with the highest and lowest axle loads were used in two simulations in order to obtain local extreme stress values.

4.3.6. Effect of clamping stress and friction coefficient on un-cracked models

A first sensitivity analysis was performed in order to evaluate the influence of clamping stress and friction coefficient. Fig. 18a) illustrates the von Mises stresses and the deformation obtained for the instant when the stresses are highest for the scenario of no

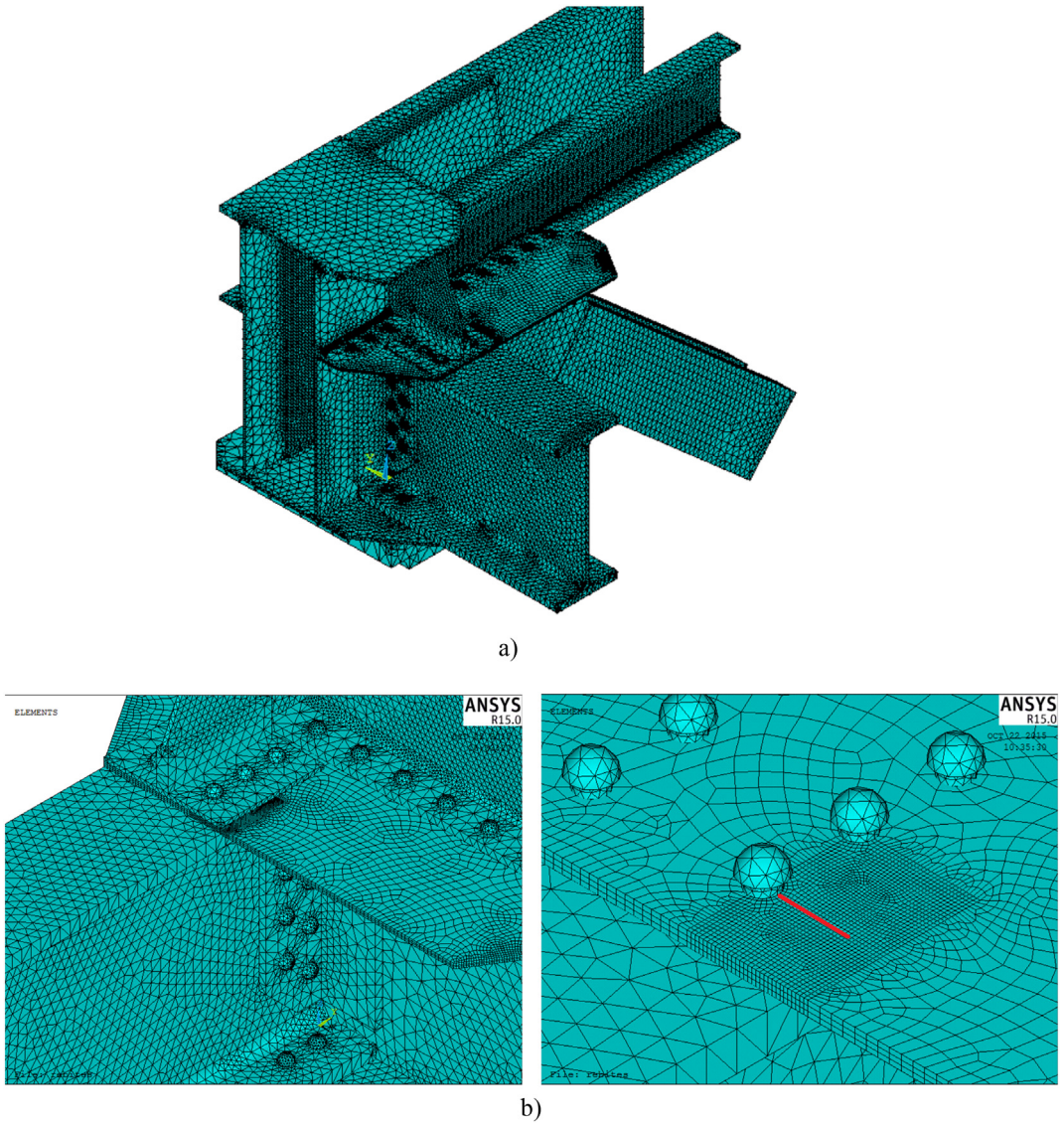

Fig. 15. Local FEM mesh: a) global view; b) local view of the rivets and crack location (one component removed to allow the crack view).

clamping stress on rivets and a friction coefficient of μ = 0.3. It is possible to observe that there is a separation between the gusset plate and the upper flange of the cross-girders in some specific instant due to important distortional effects. For the cross girder, the maximum stress concentration factor is observed at the location of the first row of rivets as can be observed in Fig. 18b).

The stress concentration factor was calculated at the top plate (horizontal gusset) connecting the top flange of the cross-girder and the upper structural elements at the location of the first row of rivets as presented in top of the Fig. 19. In this figure, the influence of the clamping stress on the stress concentration factor can be observed. It is possible to conclude that the *SCF* decreases with increasing clamping stress and stabilizes towards a value approximately equal to 1.0. This may indicate that for these clamping forces, the steel plates and the rivet behave as a single solid.

In Fig. 20, the effects of clamping stress on the stress concentration factor as a function of position to the side of the plate. In this figure, x stands for the position where the *SCF* is calculated and th is the distance between the hole of the rivet to the side of the plate. Observing these results, it is possible to conclude that the *SCF* decreases slightly faster as the clamping stress increases. This may be related to the decreasing contact forces between the shaft of the rivet and the connecting plates. These contact forces are localized and may be the main source of stress concentration.

In Fig. 21, the effect of the friction coefficient variation on the stress concentration factor can be observed for a clamping stress σ_{clamp} = 300 MPa. It is possible to conclude that the *SCF* decreases with increasing friction coefficient since load transfer by friction between the adjoining plates increases.

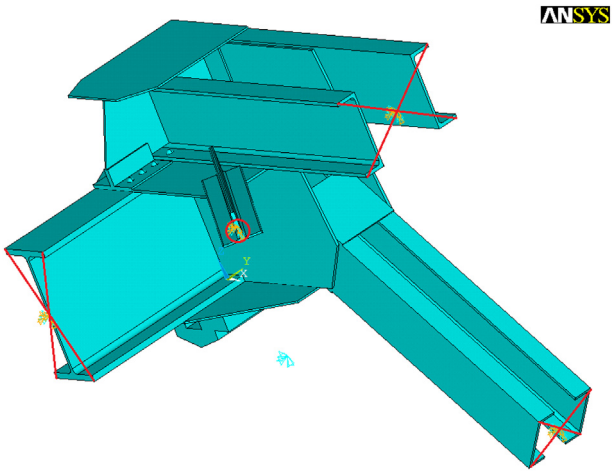

Fig. 16. Geometry of the local model and location of the multipoint constraints used to apply the displacements and rotations.

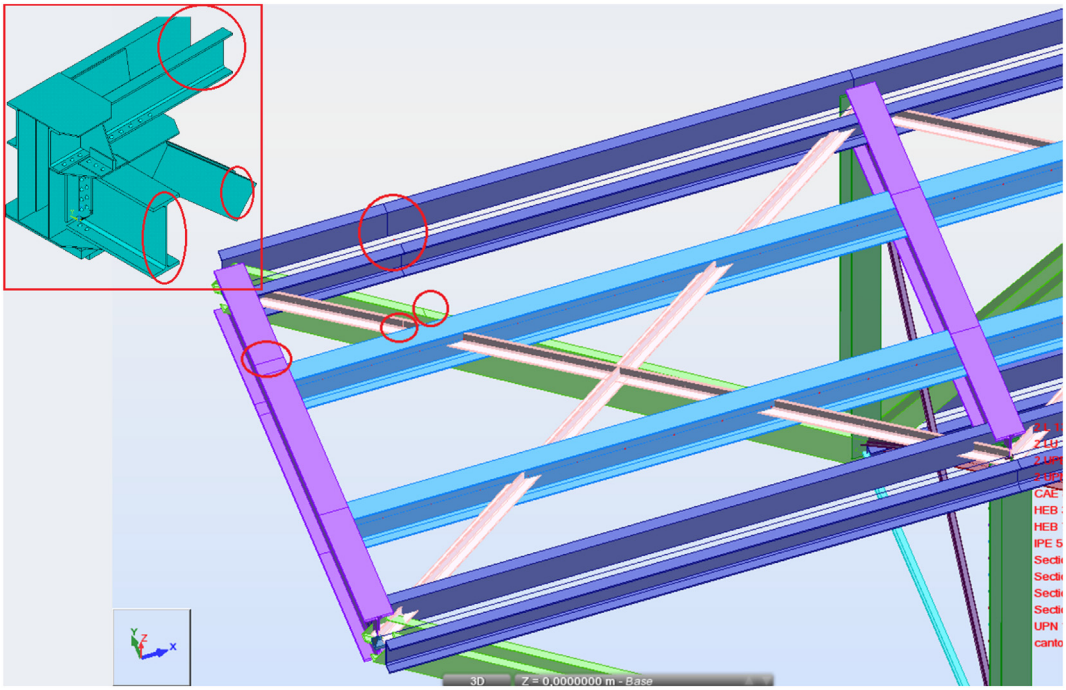

Fig. 17. Correspondence between local and global finite element models.

4.3.7. Crack growth simulation

A crack was explicitly simulated in the finite element model at the gusset plate, at the location where the Von Mises stresses were observed to be higher. Besides the higher stresses, the fatigue failure of this location is foreseen in the design codes such as the EN1993–9 standard (Fatigue class 71 for bolted connections and also recommend for riveted details) and the British standard (suggested fatigue category D, for riveted details). Furthermore, laboratory tests were developed in [31] and allowed the identification of the potential crack location. An APDL code was developed in Ansys environment in order to automatically simulate the fatigue crack growth taking into account a crack branching procedure. Crack increments of $\Delta a = 0.1$ mm were chosen. In Fig. 22a), an example of a simulated crack propagation path can be observed.

The crack propagation occurred in the direction perpendicular to the maximum principal stress. This is a direct consequence of the consideration of a crack branching criteria. In other studies previously referred, the crack propagation is stopped when the stress intensity factor calculated reach the material toughness. However, in this case, the crack was propagated further in order to allow a complete characterization of the shape function for higher values of toughness and thus include the simulations where the random variable K_c has higher values.

Fatigue cracks propagating in these complex structural details, under complex loading histories, are very likely subjected to

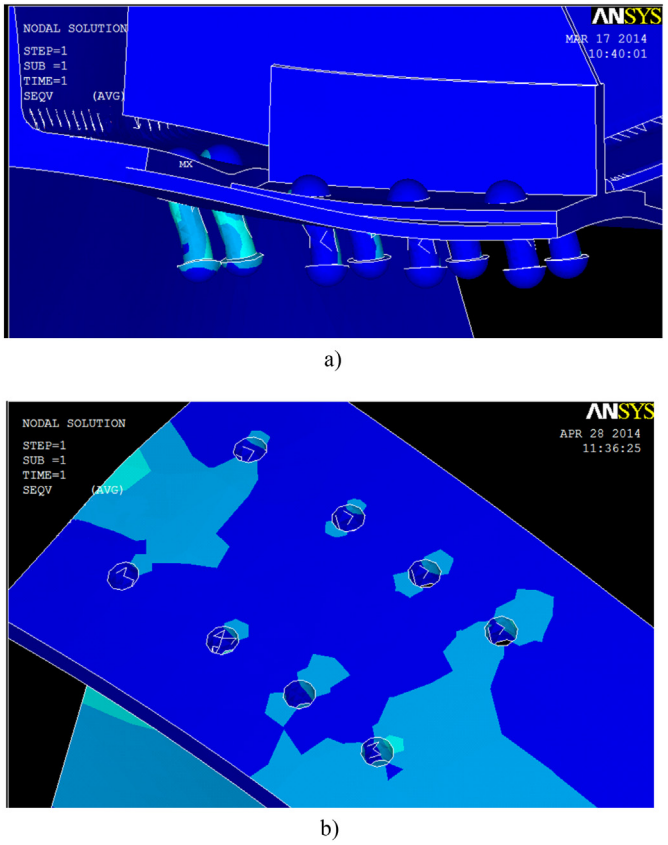

Fig. 18. Von Mises stress field resulted from the local model superimposed to the magnified deformation: a) in the rivets and in the upper part of the model; b) in the top flange of the cross-girder.

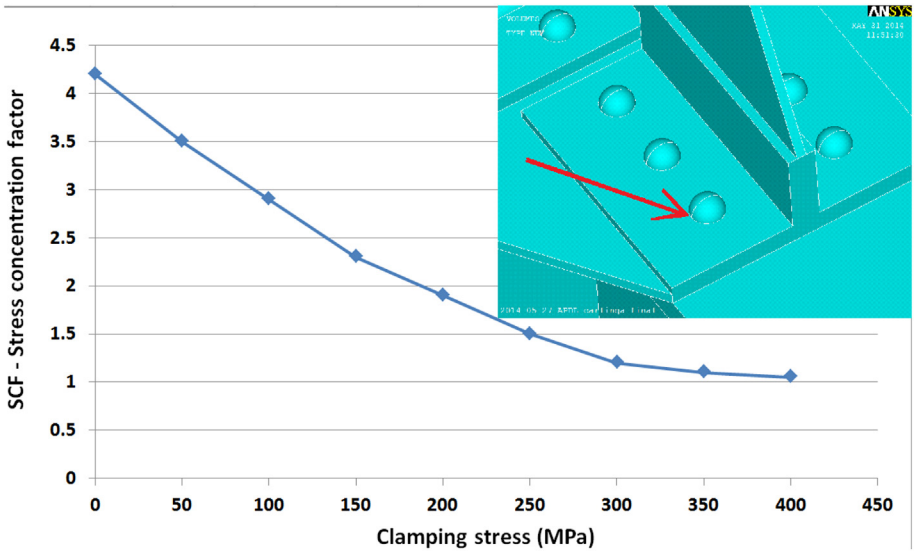

Fig. 19. Effect of clamping force on SCF on un-cracked model (μ = 0.3).

mixed-mode loading conditions. Assuming at least in plane deformation, two combined deformation modes are present: mixed (I + II) fatigue crack propagation [40]. In this case, the Paris relation may be applied using an equivalent stress intensity factor as proposed in [41–43]:

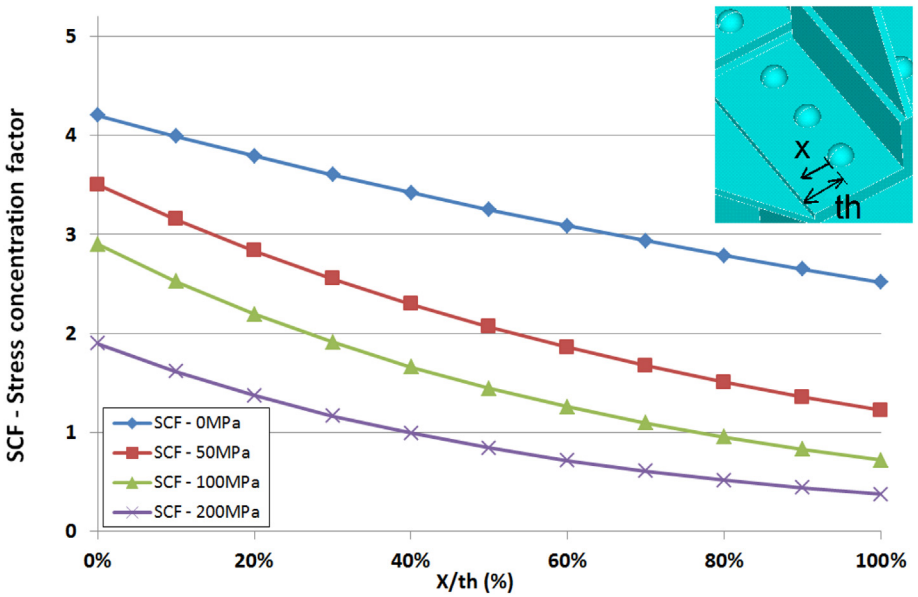

Fig. 20. Effect of clamping force on *SCF* vs. x/th ($\mu = 0.3$).

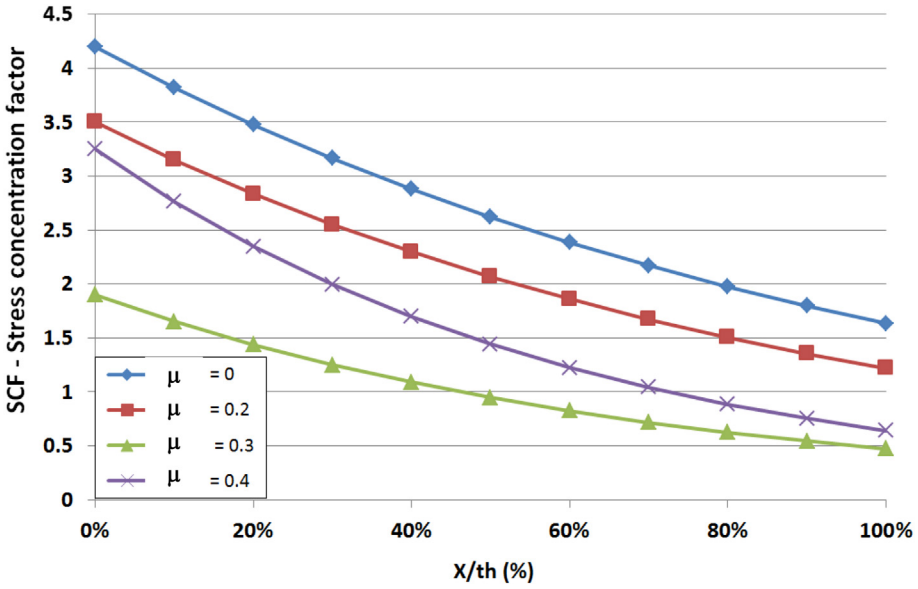

Fig. 21. Effect of friction coefficient on *SCF* on un-cracked model ($\sigma_{clamp} = 300$ MPa).

$$K_{eq} = K_I \frac{3\cos\left(\frac{\theta}{2}\right) + \cos\left(\frac{\theta}{2}\right)}{4} + K_{II} \frac{-3\sin\left(\frac{\theta}{2}\right) - 3\sin\left(\frac{3\theta}{2}\right)}{4} \tag{15}$$

where K_I is the stress intensity factor for mode I and K_{II} is the stress intensity factor for mode II.

The shape functions obtained for two trains (see references [9, 23]) are presented in Fig. 23. The two trains selected in this study and presented in references [9, 23], having the following characteristics:

- Train 1: locomotive 4700 with 15 freight wagons carrying cement, sand and wood (maximum load per axle equal to 32 ton, total load equal to 1590 ton, speed equal to 87.5 km/h, and sampling frequency equal to 100 Hz);
- Train 2: locomotive UTE 2240 with 3 carriages (maximum load per axle equal to 13.4 ton, total load equal to 155 ton, speed equal to 90.4 km/h, and sampling frequency equal to 100 Hz).

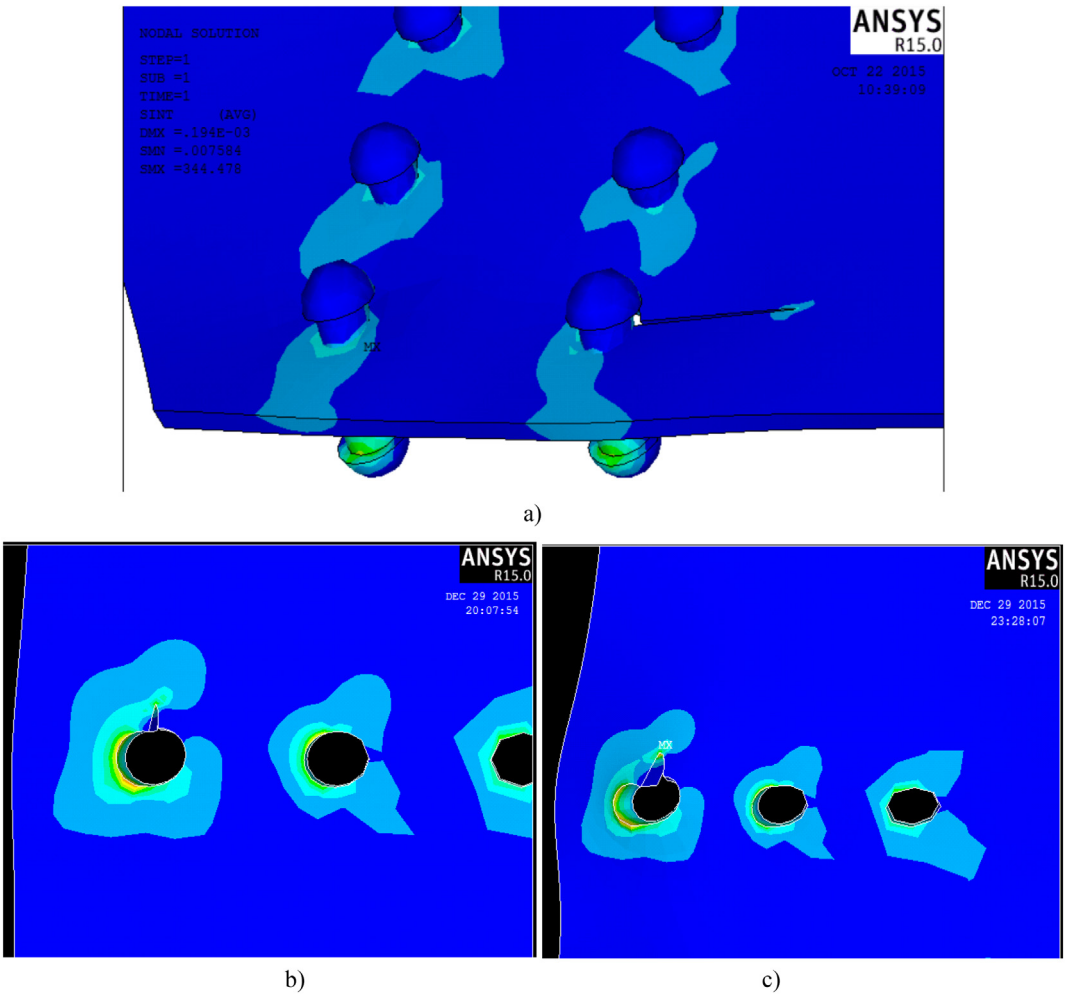

Fig. 22. Von Mises stresses in a partial view of the model: a) complete crack path; b) and c) intermediate crack configurations.

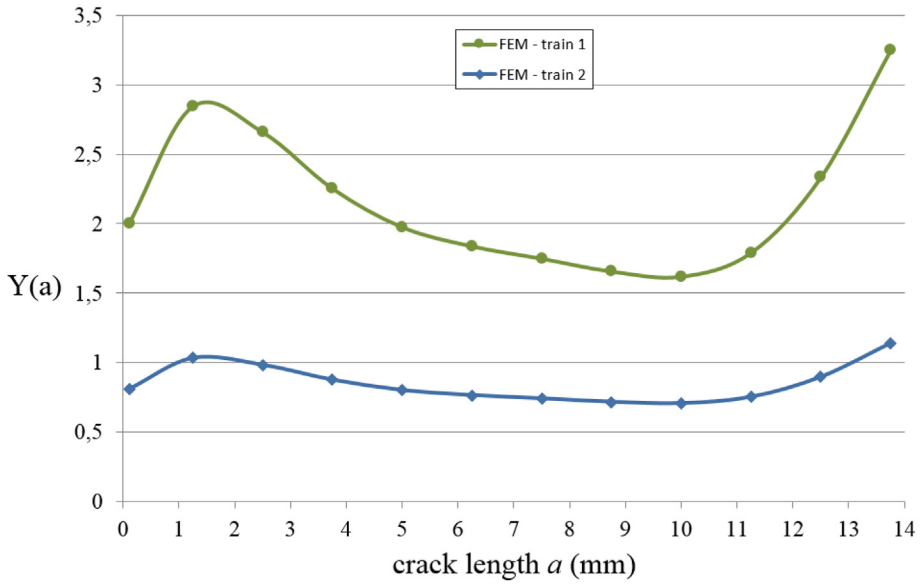

Fig. 23. Shape functions calculated from the local finite element model for two extreme trains.

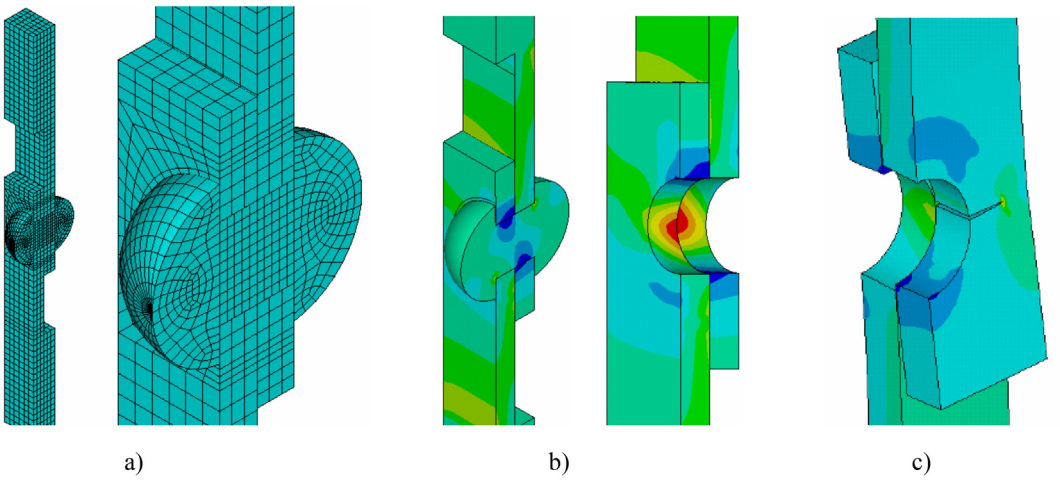

Fig. 24. 3D Finite Element model of a riveted joint: a) overview of the mesh; b) stress concentrations due to an axial load in the absence of a crack; c) final stage of the numerical crack growth simulation [17, 22].

4.3.8. Shape function analysis

In this section, a comparison is made between the shape functions obtained in this work with other studies. The first shape function considered was obtained from the work developed by Correia et al. [17] [22]. In that study, a local finite element model of a riveted joint was developed. Two independent steel plates and the corresponding rivet connecting them were modelled with volume finite elements as reproduced in Fig. 24a). The stress pattern obtained is presented in Fig. 24b) where it is possible to observe the maximum positive stresses (tension) and the minimum negative stresses (compression) both in the steel plates and in the rivet. In this case, since a linear crack was simulated, the average stress intensity factor along the thickness of the plate was calculated by the authors.

Furthermore, the same author developed another simulation with an elliptic crack [22] as presented in Fig. 25. For each crack increment, the stress intensity factors were calculated and plotted against the crack length. In this case, the two values of the stress intensity factor were calculated in accordance with the two main directions of the elliptical crack, controlling the dimensions, a and b.

A comparison between the shape functions calculated from the simulations and the ones obtained from research previously referred are presented in Fig. 26. Polynomial equations of the 6th order were fitted to all shape functions in order to use them in subsequent calculations.

It can be observed that the values of each shape functions are similar. However, the variability may have important influence in the crack growth results. If the shape function is calculated using all the real trains that crossed the bridge during the measurement period, it is assumed a combination between the shape functions obtained for “train 1” and “train 2” (see Fig. 23). Due to computational limitations, it is impossible to calculate the shape function using all measured trains combined with a non-linear finite

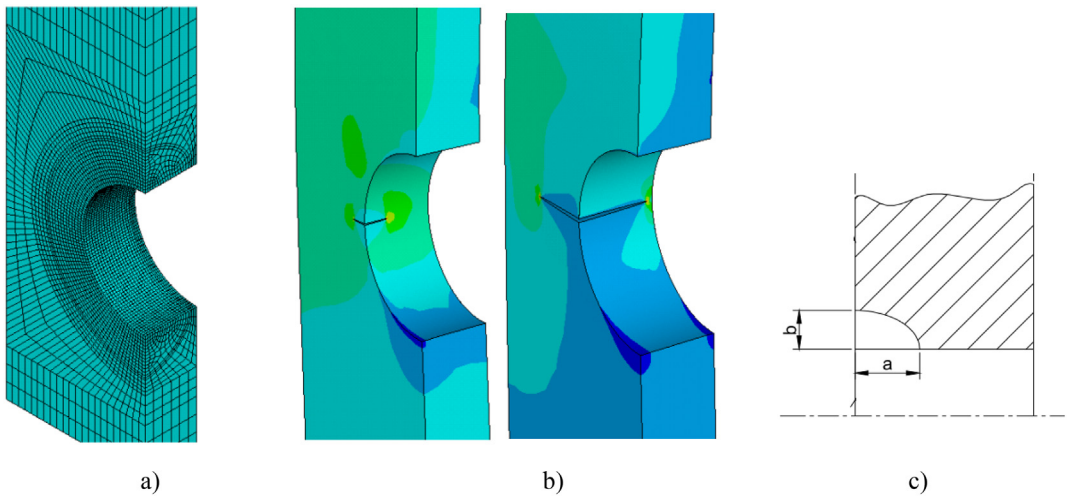

Fig. 25. 3D Finite Element model of a riveted joint with corner elliptical crack: a) partial view of the mesh; b) intermediate crack increments c) shape of the crack [17] [22].

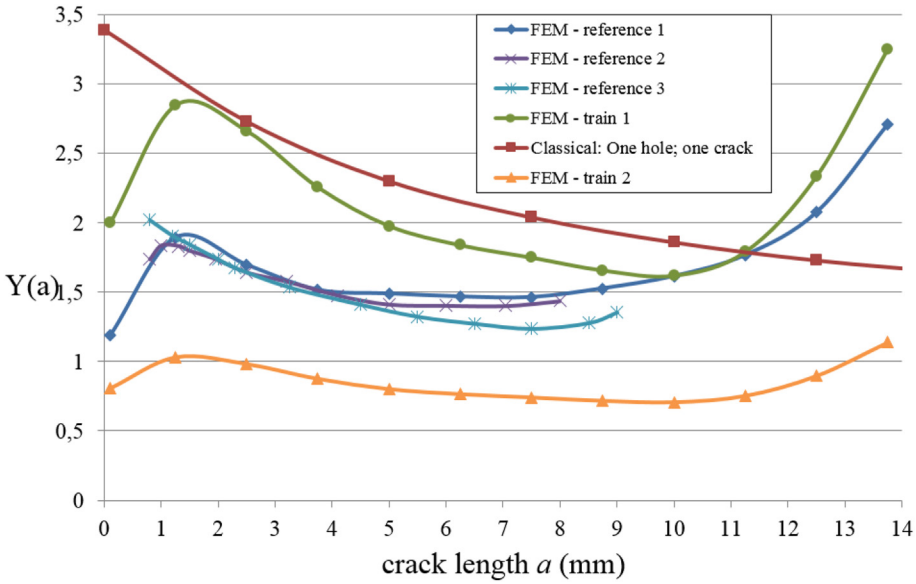

Fig. 26. Comparison between crack shape functions.

element model [42, 43]. Therefore, a genetic algorithm was implemented in order to minimize the fatigue life changing the shape function parameters. The seven parameters of the equations fitted to these results were randomly generated and their influence was analysed in Section 4.4.

4.4. Simulation of the crack growth using Monte Carlo simulation

4.4.1. Influence of the number of simulations

A sensitivity analysis was performed in order to conclude about the adequate number of simulations to be used in this research. Four different scenarios were tested, which are related to the number of Monte Carlo simulations: 2500, 5000, 10,000 and 100,000 simulations. For the purpose of this sensitivity analysis, an annual traffic growth of 5% was assumed. However, further considerations were done regarding this assumption and other annual traffic growth rates were studied.

In Fig. 27, the values of the fatigue life and the corresponding histogram are presented for the scenario taken as reference (100,000 simulations).

It is possible to observe that the range of the fatigue life obtained is coherent with the years that the bridge is in service (57 years). Furthermore, small values of fatigue life are observable which can be related to a combination of high initial crack lengths and low

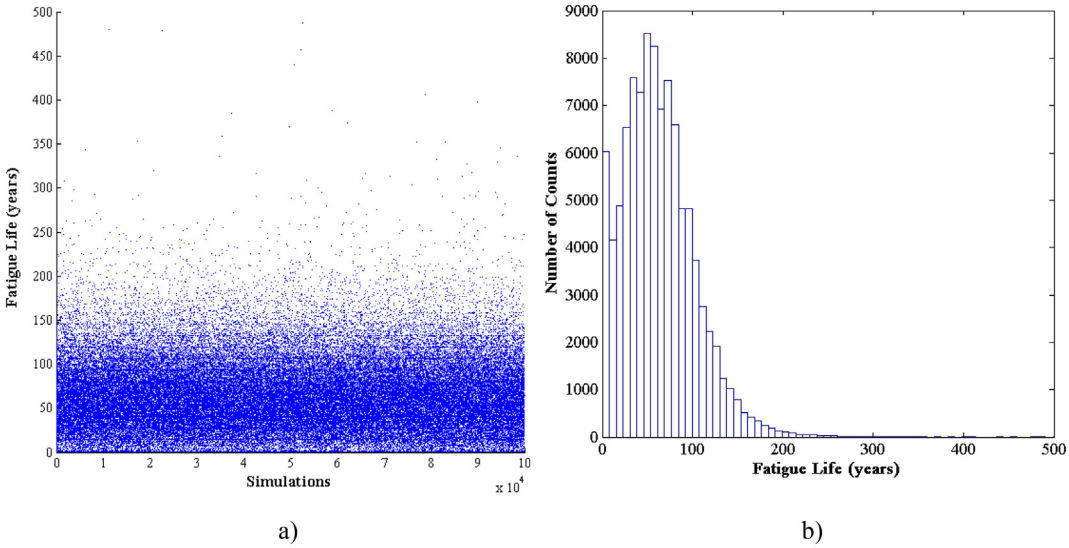

Fig. 27. Fatigue life predictions: a) results for 100,000 simulations using Monte Carlo; b) histogram of fatigue lives.

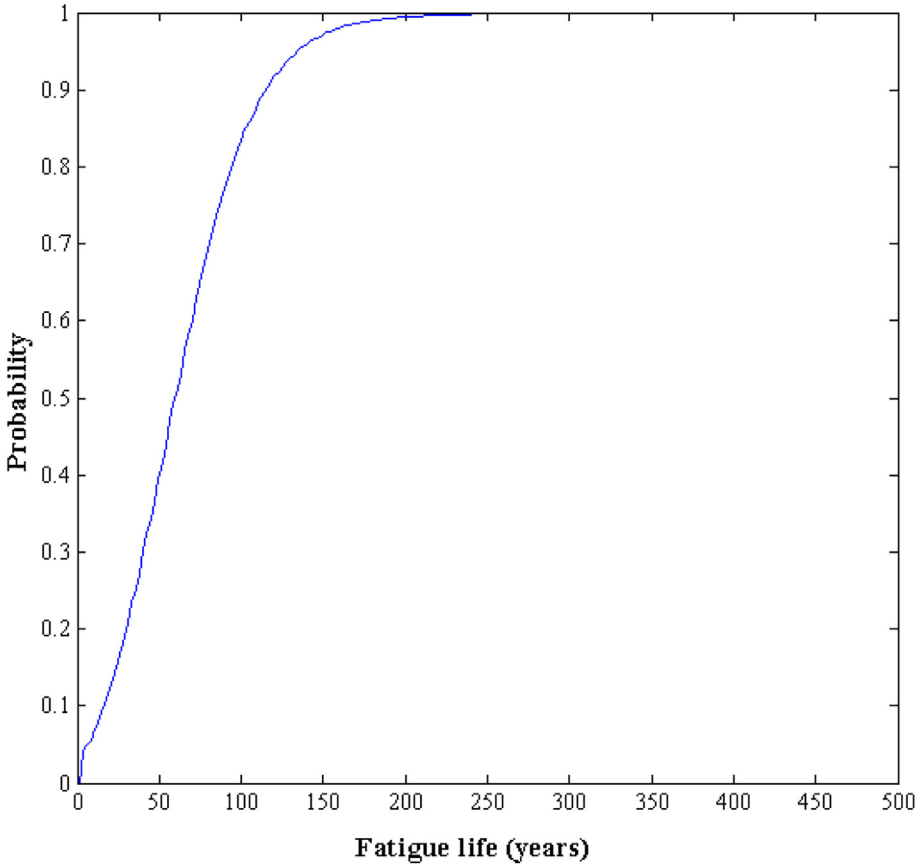

Fig. 28. Fatigue life cumulative distribution function.

critical crack lengths. In Fig. 28, the cumulative distribution function of the fatigue life is presented. Using this information it is possible to calculate the corresponding failure probability associated with a certain fatigue life or the reliability index. This kind of information is extremely useful in the decision processes that the railway administration have to make in order to choose a repair intervention or a substitution of the bridge.

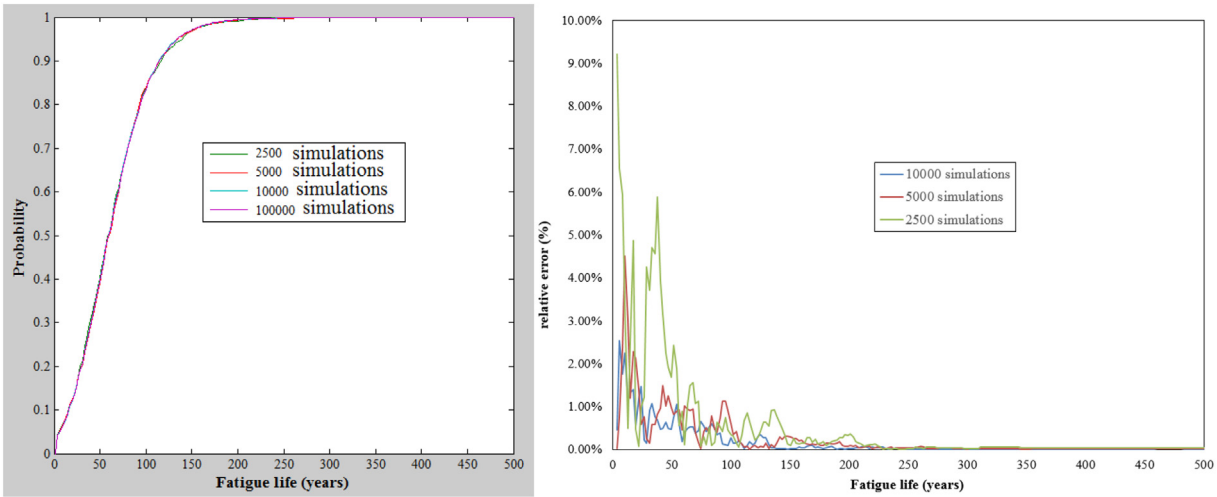

Fig. 29. Comparison of CDF of fatigue life: a) different simulation scenarios; b) relative errors.

Table 2
Minima and maxima of parameters of the shape function $Y(a)$.

Parameter	Minimum	Maximum
c1	−1.93E-04	−4.82E-05
c2	2.30E-03	4.45E-03
c3	−4.20E-02	−4.00E-02
c4	1.15E-01	3.74E-01
c5	−1.65E+00	−8.48E-01
c6	7.85E-01	2.92E+00
c7	2.01E+00	3.03E+00

In Fig. 29a, a comparison of de CDF of the fatigue life is made and in Fig. 29b) the relative error using as reference the results for 100,000 simulations.

Observing these results, a small difference is observed between the simulation scenarios for the case of higher fatigue lives. However, for smaller fatigue lives the maximum difference is approximately 9% for 2500 simulations. Taking these results into consideration, the chosen scenario for future studies is 10,000 simulations since the maximum relative error for this case is 2.54%.

4.4.2. Influence of the shape function on the critical crack length

Sixth degree polynomial equations were fitted to the shape functions calculated with the local finite element model for the case of two trains and for shape functions obtained in literature [17, 22]:

$$Y(a) = c1 \cdot a^6 + c2 \cdot a^5 + c3 \cdot a^4 + c4 \cdot a^3 + c5 \cdot a^2 + c6 \cdot a + c7 \tag{16}$$

The parameters *c1* to *c7* of Eq. (16) were then evaluated and their value was randomly generated in order to estimate the critical crack length. In this section, the influence of the shape function on the critical length is evaluated. In Table 2, minimum and maximum values of the parameters of the shape function are presented.

Four example histograms of the critical crack length with a fitted normal distribution are presented in Fig. 30.

The corresponding shape functions are presented in Fig. 31.

It is relevant to notice that the values of the critical crack length have high variability. This may lead to important variations in the

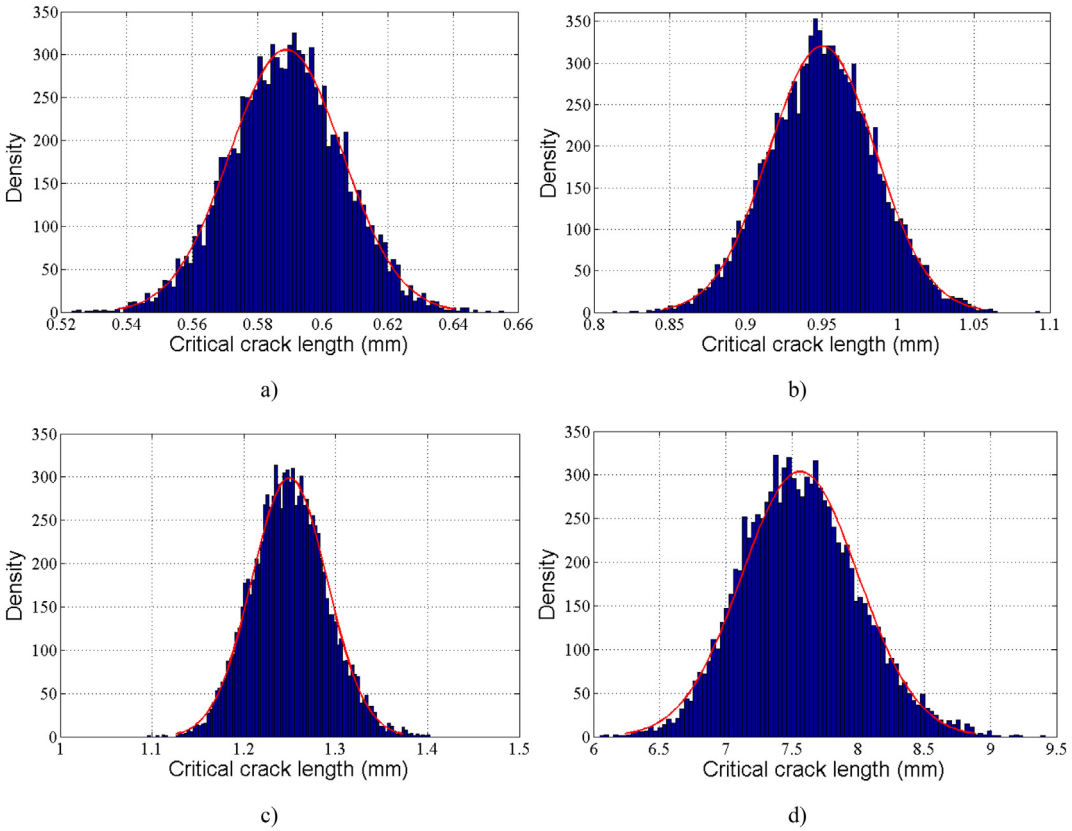

Fig. 30. Critical crack length: a) shape function 4; b) shape function 2; c) shape function 3; d) shape function 1.

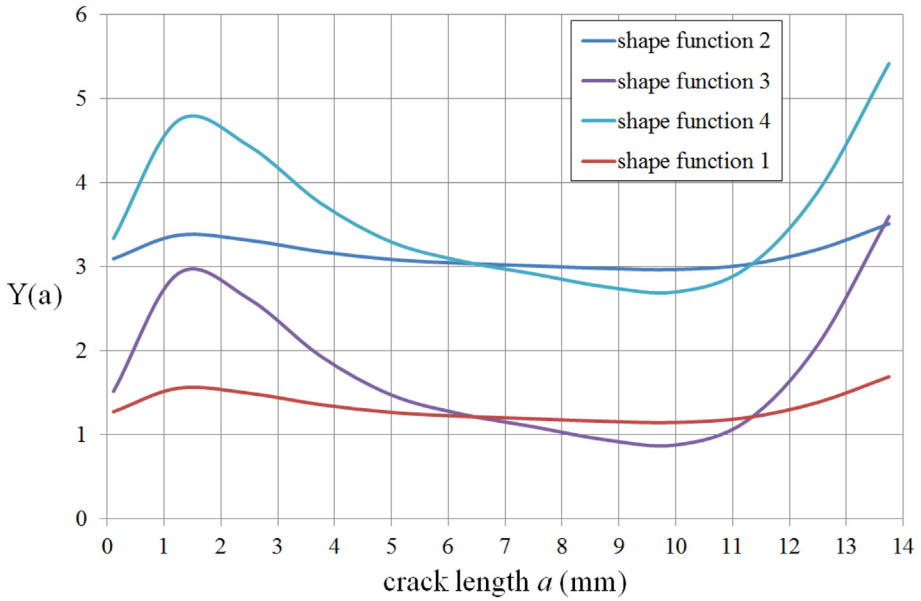

Fig. 31. Four examples of shape functions randomly generated.

fatigue life. Lower crack lengths and their corresponding shape functions correspond to lower fatigue lives. However it is not possible to conclude in advance which is the shape function leading to lowest fatigue lives. This is due to the non-linearity of the shape functions, non-linear relation with the critical crack length and with the Paris law [8].

4.4.3. Load function sensitivity analysis

As referred previously, since the number of trains to failure is very high and to reduce computational time, it is necessary to employ the central limit theorem (CLT) of probability to aggregate several trains crossing into each loading block. In this context, a sensitivity analysis was made to conclude about the correlation between the fatigue life and the number of trains in each loading block. For that purpose, all the remaining random variables were assumed constant and with their mean value.

In Fig. 32, it is possible to observe that the relative error of the fatigue life is small for all the traffic scenarios bellow the monthly traffic scenario. Above this number of trains included in the calculation of the damage stress function, the relative error increases significantly. Therefore, taking into account this conclusion, the monthly traffic was used in this work.

4.4.4. Traffic growth

The influence of annual traffic growth can be observed in Fig. 33. In order to develop a sensitivity analysis, all the parameters of the model (C, m, a_{ini}, K_{ic} and m) were considered deterministic and equal to their mean value. Their mean value was adopted and the probability distribution presented in Fig. 10 was used for the stress damage function.

As can be seen, the fatigue life reaches very high values when the annual traffic growth equal to zero is considered. This scenario

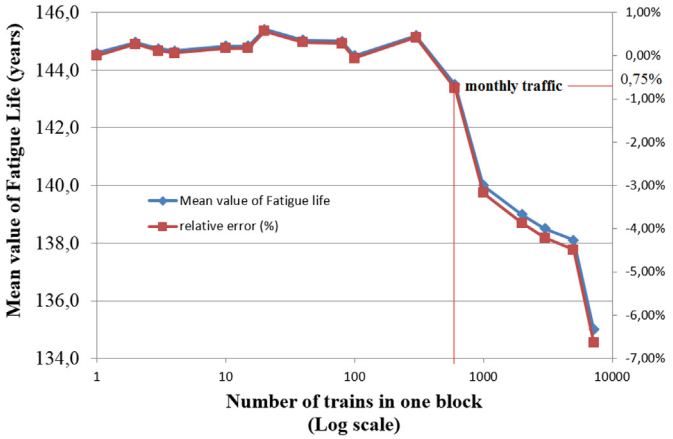

Fig. 32. Number of train crossings in the loading block vs. fatigue life.

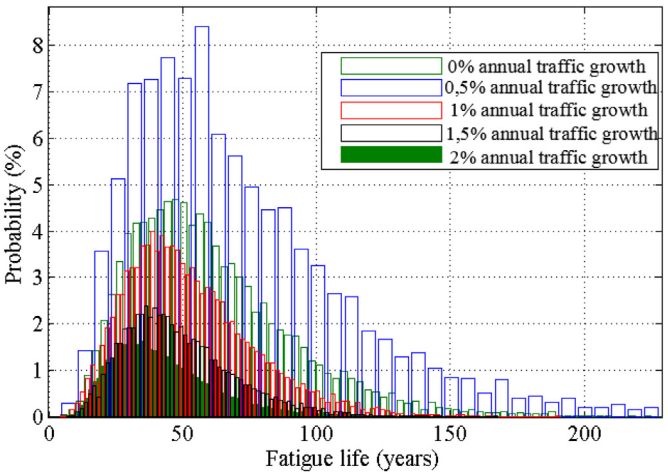

Fig. 33. Histograms of fatigue life taking into account several traffic growth rates.

is unrealistic, because it is known that, normally, there is traffic growth associated with the number of trains in service. Based on the histograms calculated, it is possible to evaluate the failure probability in correspondence with the value of the fatigue life by calculating the cumulative distribution functions. In Fig. 34, the results of the simulations for the annual traffic growth equal to 0%, 0.5%, 1% and 2% are shown.

As can be observed, there is an important influence of annual traffic growth on the value of fatigue life. For example, a probability of failure of 50% corresponds to fatigue lives of approximately 60 years and 40 years respectively for 0% and 2% annual traffic growth.

4.4.5. Critical shape function for fatigue life assessment

The shape function which corresponds to the lowest fatigue life (critical shape function) was evaluated in this section using a genetic algorithm. In Fig. 35a) the fatigue life is plotted against the generation number. As can be observed, the total number of generations chosen for this analysis is adequate since the difference between the best fit and the mean fit is very small (0.09 years). In Fig. 35b), the average distance between each individuals, which are the group of values which characterize the shape function (see Table 2), are also plotted against the generation number. It can be observed that for the last generation, this average distance is almost zero leading to good results of the optimization.

As can be observed, the minimum fatigue life obtained is 67.08 years. This is the value of the total fatigue life for the worst shape function obtained as a combination of the shape functions presented in Section 4.3.8 and if all the parameters of the model remained constant since the inauguration of the bridge. The critical shape function corresponding to this minimum value of the fatigue life (100th generation) is presented in Fig. 36 and referred as *y100*. Intermediate shape functions derived from the optimization steps 1, 30 and 60 and the shape functions calculated for train 1 and train 2 (Section 4.3.7) are also presented for comparison purposes. The constants of the critical shape function are also presented in this figure.

As already stated, in order to represent the real behaviour of the cracked detail loaded by real trains, this shape function must be

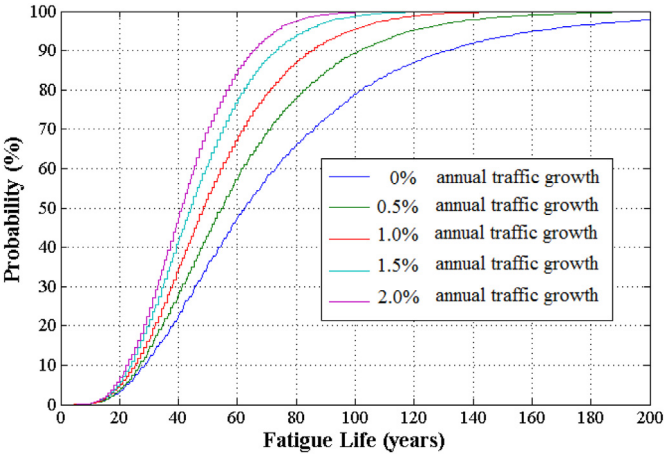

Fig. 34. Cumulative distribution function of fatigue life taking into account several traffic growth rates.

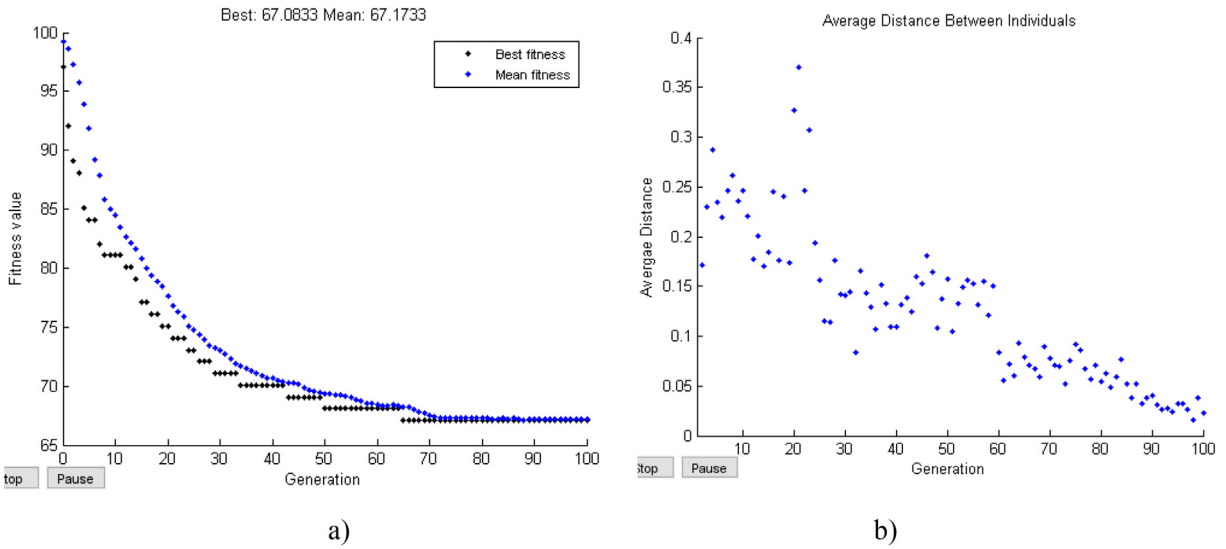

Fig. 35. Minimization of the fatigue life by changing the shape function parameters: a) Fitness value (fatigue life) vs. generation number; b) average distance between individuals vs. generation number.

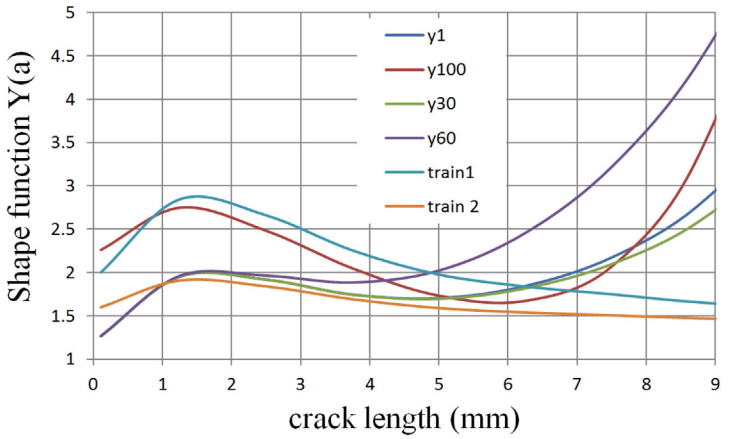

y100	c1	c2	c3	c4	c5	c6
	-2.0102E-05	1.1047E-03	-1.8869E-02	1.6193E-01	-7.1084E-01	1.1550E+00

Fig. 36. Critical shape function *y100* for the evaluation of fatigue life compared with intermediate shape functions.

related to the shape functions calculated numerically in Section 4.3.8.

5. Conclusions

In this paper, in order to provide more reliable alternative tools than the conventional blind and over conservative S—N approaches, Fracture Mechanics concepts were implemented. Several Matlab routines were developed to implement a methodology based on integration of Paris law together with the concept of random block loading and Monte Carlo sampling technique. Several influencing parameters were considered random variables besides the stress ranges, such as the crack initiation size, the critical crack size, the geometric shape functions used to compute the stress intensity factors for propagating cracks.

Several numerical sensitivity analyses were performed. The first sensitivity analysis allowed to conclude that, in this case, 10,000 sampling simulations are enough to estimate the fatigue life with good accuracy. Furthermore, the annual traffic growth has a very important influence on the results of the fatigue life. Therefore, special attention must be given to the definition of this variable. In this context, a traffic growth of 1% per year was adopted as proposed in literature. It is also essential to choose an adequate shape function to calculate the fatigue life. This was demonstrated by a sensitivity analysis on the critical crack length.

Since it is impractical to calculate local cracked models with non-linear behaviour loaded with the real stress spectra from measurements obtained from the long term monitoring campaign, a new approach was proposed to implement local fatigue analysis.

Several shape functions were calculated based on the local numerical model developed and were compared with the shape functions obtained from literature. Due to the non-linear nature of the problem, a genetic algorithm was implemented in order to minimize the fatigue life by changing the shape function parameters. Adopting this approach, it is possible to obtain a critical shape function for fatigue evaluation. Since the resulting function is a combination of real, calculated ones, it is also a realistic shape function.

References

[1] B. Kuhn, M. Lukić, A. Nussbaumer, H.-P. Guenther, R. Helmerich, S. Herion, et al., Assessment of existing steel structures: recommendations for estimation of remaining fatigue life, Joint Res. Centre 1 (2008) 1–90.
[2] ASCE, Committee on fatigue and fracture reliability of the committee on structural safety and reliability of the structural division, fatigue reliability: 1–4, J. Struct. Eng. ASCE (1982) 3–88.
[3] A.M.P. De Jesus, H. Pinto, A. Fernández-Canteli, E. Castillo, J.A.F.O. Correia, Fatigue assessment of a riveted shear splice based on a probabilistic model, Int. J. Fatigue 32 (2010) 453–462.
[4] A.M.P. De Jesus, M.A.V. Figueiredo, A.S. Ribeiro, P.M.S.T. De Castro, A.A. Fernandes, Residual lifetime assessment of an ancient riveted steel highway bridge, Strain 47 (1) (2011) e402–e415.
[5] C.S. Horas, J.A.F.O. Correia, A.M.P. De Jesus, P. Kripakaran, R. Calçada, Application of the modal superposition technique combined with analytical elastoplastic approaches to assess the fatigue crack initiation on structural components, Eng. Fract. Mech. 185 (2017) 271–283.
[6] M. Miguel Muñiz-Calvente, A.M.P. De Jesus, J.A.F.O. Correia, A. Fernández-Canteli, A methodology for probabilistic prediction of fatigue crack initiation taking into account the scale effect, Eng. Fract. Mech. 185 (2017) 101–113.
[7] M. Matsuishi, T. Endo, Fatigue of Metals Subjected to Varying Stress, Japan Soc. Mech. Engineering, 1968.
[8] F. Erdogan, P. Paris, A critical analysis of crack propagation laws, J. Basic Eng. Trans. Am. Soc. Mech. Eng. (1963) 528–534.
[9] F.M.S. Marques, Fatigue Assessment of Old Riveted Railway Bridges, University of Porto, 2016 (Ph.D. thesis, 256 pages).
[10] M.A. Miner, Cumulative damage in fatigue, J. Appl. Mech. 12 (1945) 159–164.
[11] EN 1993-1-9, Eurocode 3: Design of Steel Structures - Part 1–9: Fatigue Fatigue Strength of Steel Structures, European Comitte for Standardization, Brussels, 2005.
[12] P.J. Massareli, T.T. Baber, Fatigue Reliability of Steel Highway Bridge Details, Virginia Transportation Research Council, August 2001.
[13] ASTM, E1049–85(2017), Standard Practices for Cycle Counting in Fatigue Analysis, ASTM International, West Conshohocken, PA, 2017, https://doi.org/10.1520/E1049-85R17.
[14] Ribeiro, A., et al., Avaliação da integridade estrutural da ponte de Trezói. Portuguese Research Project Report, “Avaliação da Integridade Estrutural de Pontes Metálicas Ferroviárias”.
[15] American Society for Testing and Materials, Constant-Load-Amplitude, Fatigue crack growth rates above 10–5 m/cycle, Annual Book of ASTM Standards, Part. 10, E647–82, 1982.
[16] P. Raposo, J.A.F.O. Correia, G. Lesiuk, I. Valente, A. Jesus, R. Calçada, Mechanical characterization of ancient Portuguese riveted bridges steels, Eng. Struct. Technol. 9 (4) (2017) 169–180.
[17] J.A.F.O. Correia, A.M.P. De Jesus, A.L.L. Silva, B. Pedrosa, C. Rebelo, R. Calçada, FE simulation of S-N curves for a riveted connection using two-stage fatigue models, Adv. Comput. Des. Int. J. 2 (4) (2017) 333–348.
[18] P. Albrecht, N. Yazdani, Risk analysis of extending bridge service life, Report no. FHWA/MD-84/01, University of Maryland, 1986.
[19] F.V. Lawrence Jr., R.J. Mattos, Y. Higashida, J.D. Burk, Estimation the fatigue crack initiation life of welds, in: D.W. Hoeppner (Ed.), Fatigue Testing of Weldments, ASTM STP 648, American Society for Testing and Materials, 1978, pp. 134–158.
[20] H. Jakubczak, G. Glinka, Fatigue analysis of manufacturing defects in weldments, Int. J. Fatigue 8 (2) (1986) 51–57.
[21] A.S. Ribeiro, Effect of the Crack Initiation Phase on the Fatigue Behaviour of Welded Joints (Ph.D. Thesis, in Portuguese), University of Trás-os-Montes e Alto Douro, Portugal, 1993.
[22] J.A.F.O. Correia, Desenvolvimento de modelos de previsão da vida à fadiga de ligações rebitadas, UTAD, 2008 (Master thesis, in portuguese).
[23] F. Marques, C. Moutinho, W.H. Hu, A. Cunha, E. Caetano, Weigh-in-motion implementation in an old metallic railway bridge, Eng. Struct. 123 (2016) 15–29.
[24] M. Rosenblatt, Remarks on some nonparametric estimates of a density function, Ann. Math. Stat. 27 (3) (1956) 832, https://doi.org/10.1214/aoms/1177728190.
[25] H. Tada, P.C. Paris, G.R. Irwin, The Stress Analysis of Cracks Handbook, Professional Engineering Publishing, 2000.
[26] B.M. Imam, T.D. Righiniotis, M.K. Chryssanthopoulos, Numerical modelling of riveted railway bridge connections for fatigue evaluation, Eng. Struct. 29 (2007) 3071–3081.
[27] R.C. Guyer, J.A. Laman, Distortion-induced stress investigation of double angle stringer-to-floorbeam connections in railroad bridges, Eng. Struct. 38 (2012) 104–112.
[28] C. Albuquerque, A.L.L. Silva, A.M.P. de Jesus, R. Calçada, An efficient methodology for fatigue damage assessment of bridge details using modal superposition of stress intensity factors, Int. J. Fatigue 81 (2015) 61–77.
[29] B. OS, J.P. J, Benchmarks for finite element modelling of bolted steel connections, J. Constr. Steel Res. 43 (1997) 17–42.
[30] SAS, Swanson Analysis Systems Inc, ANSYS, Houston, 2008 Version 11.0.
[31] A.M.P. De Jesus, et al., Strain-life and crack propagation fatigue data from several Portuguese old metallic riveted bridges, Eng. Fail. Anal. 18 (2011) 148–163.
[32] Wilson, W.M., Thomas, F.P., Fatigue tests of riveted joints. In Engineering Experiment Station. 1938, University of Illinois: Urbana.
[33] J.A.F.O. Correia, An Integral Probabilistic Approach for Fatigue Lifetime Prediction of Mechanical and Structural Components, University of Porto, 2014 (Ph.D. Thesis, 382 pages).
[34] L. Gallegos-Mayorga, S. Sire, J.A.F.O. Correia, A.M.P. De Jesus, C. Rebelo, A. Fernández-Canteli, M. Ragueneau, B. Plu, Statistical evaluation of fatigue strength of double shear riveted connections and crack growth rates of materials from old bridges, Eng. Fract. Mech. 185 (2017) 241–257.
[35] A.M.P. De Jesus, A.L.L. Silva, J.A.F.O. Correia, Fatigue of riveted and bolted joints made of puddle iron - an experimental approach, J. Constr. Steel Res. 104 (2015) 81–90.
[36] J. Kafie-Martinez, P.B. Keating, P. Chakra-Varthy, J. Correia, A. de Jesus, Stress distributions and crack growth in riveted lap joints fastening thick steel plates, Eng. Fail. Anal. 91 (2018) 370–381.
[37] M. Rodrigues, J.A.F.O. Correia, A.M.P. De Jesus, B. Pedrosa, B. Carvalho, C. Rebelo, J. Xavier, R.A.B. Calçada, Numerical analysis of a double shear standard bolted connection considering monotonic loadings, Eng. Struct. Technol. 9 (4) (2017) 181–192.
[38] Standarsization., C.E.C.f, EN1991-2, Eurocode 1: Actions on Structures - Part 2: Traffic Loads on Bridges, (2003).
[39] J.P. Matthew, Variable Amplitude Fatigue Analysis Using Surrogate Models and Exact XFEM Reanalysis, 2011 University of Florida, 2011.
[40] G. Lesiuk, P. Kucharski, J.A.F.O. Correia, A.M.P. De Jesus, C. Rebelo, L. Simões da Silva, Mixed mode (I+II) fatigue crack growth in puddle iron, Eng. Fract. Mech. 185 (2017) 175–192.
[41] A.L.L. Silva, A.M.P. De Jesus, J.M.C. Xavier, J.A.F.O. Correia, A.A. Fernandes, Combined analytical-numerical methodologies for the evaluation mixed-mode (I+II) fatigue crack growth rates in structural steels, Eng. Fract. Mech. 185 (2017) 124–138.
[42] J. Leander, M. Aygül, B. Norlin, Refined fatigue assessment of joints with welded in-plane attachments by LEFM, Int. J. Fatigue 56 (2013) 25–32.
[43] C.S. Horas, G. Alencar, A.M.P. De Jesus, R. Calçada, Development of an efficient approach for fatigue crack initiation and propagation analysis of bridge critical details using the modal superposition technique, Eng. Fail. Anal. 89 (2018) 118–137.